AD-A192 248 ELECTRON-IMPACT-IONIZATION AND ELECTRON-ATTACHMENT CROSS SECTIONS OF RADI (U) SAN DIEGO STATE UNIV CA DEPT OF ELECTRICAL AND COMPUTER ENGIN L C LEE ET AL 1/1

UNCLASSIFIED 05 FEB 88 N00014-86-K-0558 F/G 7/4 NL

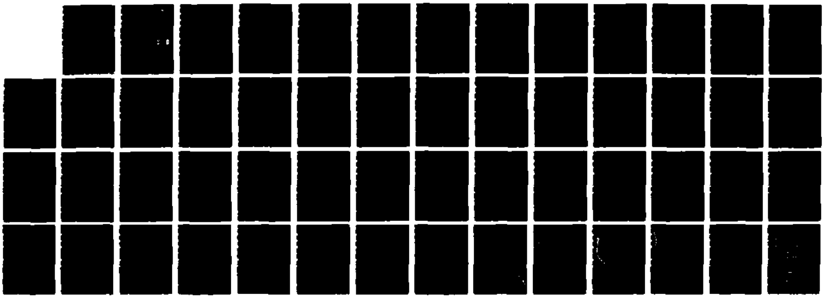

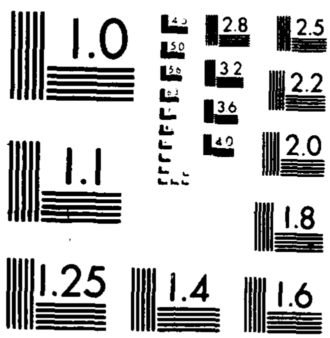
1.0
2.8
2.5
3.2
2.2
3.6
4.0
2.0
1.1
1.8
1.25
1.4
1.6

DTIC FILE COPY

February 5, 1988

AD-A192 248

Annual Report for Grant No. N00014-86-K-0558
Research project sponsored by SDIO/IST and Managed by ONR

Covering the period from September 1, 1986 to December 31, 1987.

Electron-Impact-Ionization and Electron-Attachment Cross Sections of Radicals Important in Transient Gaseous Discharges

Submitted by:

Long C. Lee and Dong P. Wang
Department of Electrical and Computer Engineering
San Diego State University
San Diego, CA 92182

Santosh K. Srivastava
Jet Propulsion Laboratory
California Institute of Technology
Pasadena, CA 91109

Prepared for:

Office of Naval Research
800 North Quincy Street
Arlington, VA 22217-5000

Attention: Dr. Bobby R. Junker
Director, Mathematical and Physical Sciences Directorate

Table of Contents

I. Introduction

This report describes the research results obtained in the period from September 1, 1986 to December 31, 1988 for the research program supported by SDIO/IST and managed by ONR under Grant No. N00014-86-K-0558. In this research program, an apparatus using electron beam, laser beam and molecular beam has been constructed to measure the electron-impact-ionization cross sections and electron-attachment cross sections of radicals that are abundant in electrical discharge media. The electron excitation cross sections of radicals are very little known. The radical data are needed for understanding the microscopic processes of electrical discharges and for designing gaseous discharge switches. High power gaseous discharge switches are currently needed for the development of inductive-energy-storage systems, high power lasers, and particle beam experiments.

In this reporting period, we have completed the construction of experimental apparatus. The performance of the apparatus was tested with electron excitations of noble gases, CO, N_2, O_2, CO_2, and CH_4, and compared with published data in the areas of ionization thresholds, excitation ionization cross sections and dissociative electron attachment processes. We found that the apparatus functions appropriately as expected. We also tested the laser effect on the electron excitation processes of molecules. Laser-enhanced ion productions were observed in N_2 and CH_3OH, but not in Ar. The mechanisms for the laser-enhanced ionization were investigated. The electron-impact ionization

cross sections of radicals and excited species will be derived from these enhanced signals once the mechanisms are understood.

The absolute electron-impact ionization cross sections of NH_3 and CH_3OH and the electron dissociative attachment cross sections of CH_3Cl, SiH_4 and CH_4 were measured at the Jet Propulsion Laboratory. These data will be used for the calibration of the absolute electron-excitation cross sections of radicals that are being measured in this research program.

II. Research Accomplished

A. Experimental Apparatus

The schematic diagram of the constructed apparatus is shown in Fig. 1. This apparatus consists of an electron beam, a molecular beam injector, an excimer laser (Lumonics excimer-510) and a quadrupole system. The vacuum chamber was pumped by a turbo-molecular pump (Balzer TSU-1500). A background vacuum pressure of 10^{-8} mbar was obtained. The typical gas pressure in the experiment was in the range of 10^{-7} mbar. The electron beam was generated by an electron gun which had about 0.5 eV FWHM (full width at half-maximum) energy resolution. The electron gun and ion extraction were of the same design of Srivastava at the Jet Propulsion Laboratory. Ions produced by electron excitation were selected by a quadrupole mass analyzer and detected by a channeltron. The output pulses from the channeltron were amplified by a preamplifier (Stanford research system SR440) and counted by a fast photon counter (SRS SR400) which had a

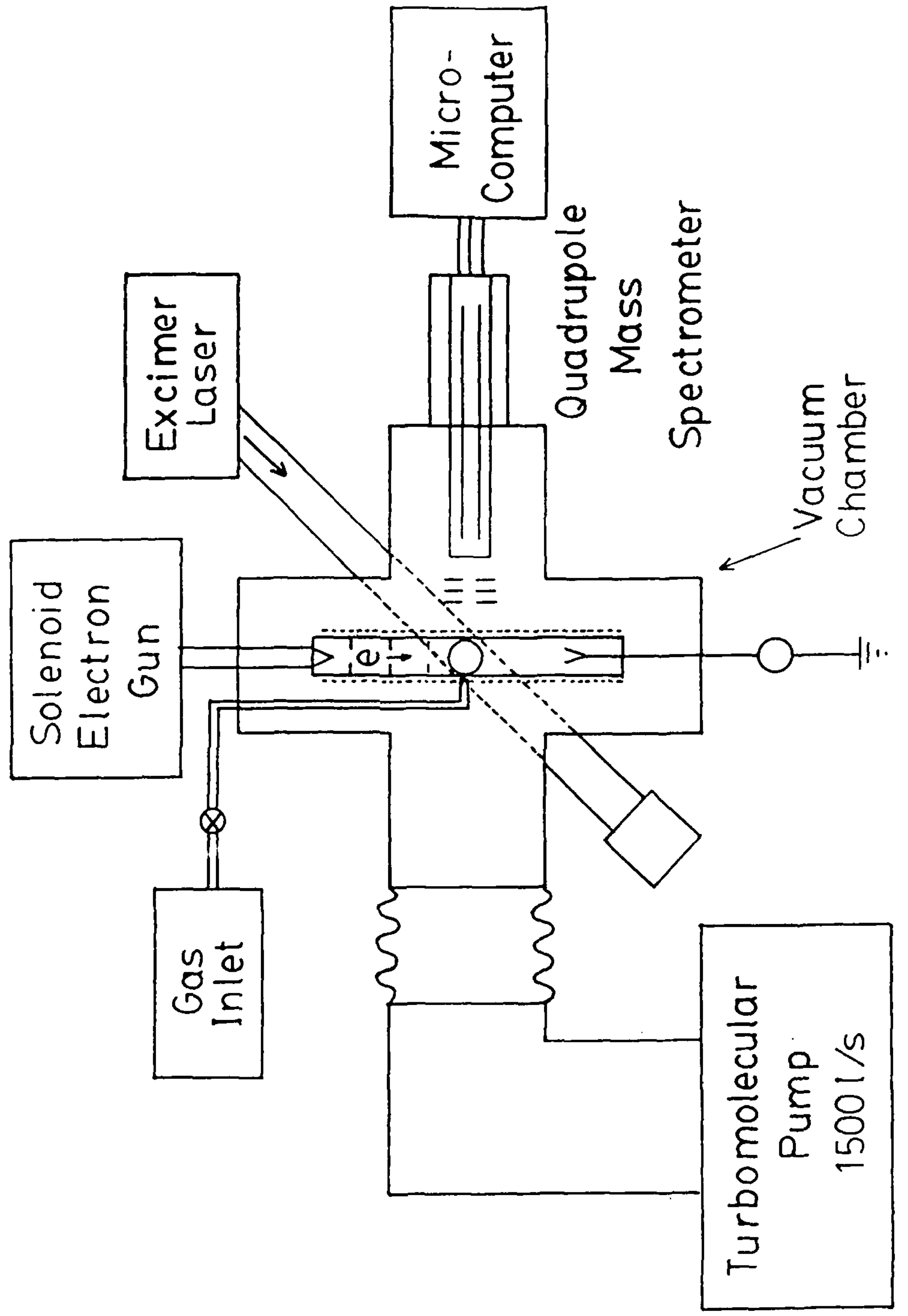

Fig. 1. Schematic diagram for the experimental apparatus

resolution of 200 MHz. The fast photon counter was controlled by an IBM PC through a RS232 connection. The data collected by the counter were transferred to the PC during the experiment. The counter and excimer laser are triggered by a pulse generator.

The electron beam energy can be scanned by a voltage output from the counter. Most of the data are accumulated by 10 scans to average over the variations of gas pressure, electron beam current and the detection efficiency of the quadrupole system. The gas was introduced into the chamber through a variable leak valve. The pressure was measured by a capacitance manometer (MKS Instruments) installed between the leak valve and the chamber. The pressure was also monitored by a cold cathode gauge which was installed about 50 cm away from the electron-gas interaction region. A linear relation between different pressure measurements was observed for most gases up to 10^{-6} mbar.

The laser beam diameter was cut down by an iris aperture of 0.32 cm. A MgF_2 window was placed on the chamber for laser entrance. The laser power was monitored by a power meter (Scientech). The laser power could be attenuated by placing in front of the MgF_2 window with different combinations of quartz and sapphire plates. The data are analyzed by Lotus 1-2-3 software that includes curve fitting.

B. Test of Apparatus Performance

The performance of the apparatus was tested by measuring the electron ionization cross sections of Ne, Ar, Kr, Xe, O_2 and N_2 in the electron energy range 10-300 eV. The electron ionization

potential energies and ionization cross sections are consistent with published data within experimental uncertainties. This ensures that the electron gun and the mass spectrometer detection system behave normally. The electron ionization processes of CH_4 were investigated in the electron energy range 0-300 eV. The primary results for the production cross sections of C^+, CH^+, CH_2^+, CH_3^+, and CH_4^+ from electron impact excitation of CH_4 were reported to ONR earlier (Letter Report submitted on July 28, 1987).

The dissociative electron attachment processes of O_2, CO and CO_2 were also studied in this reporting period. The results are consistent with published data. This ensures that this apparatus can be used to study the dissociative electron attachment processes of radicals. The primary results for the excitation function of dissociative electron attachment to CO_2 was reported to ONR earlier (Letter Report submitted on July 10, 1987).

The effect of laser irradiation on the electron excitation processes of molecules was investigated in this reporting period. The laser pulse width was about 10 ns, and the electron beam was continuous. The ion signals enhanced by laser photons would only last a short time after each laser pulse. With this time-resolved method, the laser-enhanced signal can be differentiated from the continuous background. The ion signals were measured as function of the delay time from the laser pulse. The results for the laser effect on the electron excitation of Ar and N_2 are shown in Fig. 2, where the gate was open for 115 μs, and the ArF

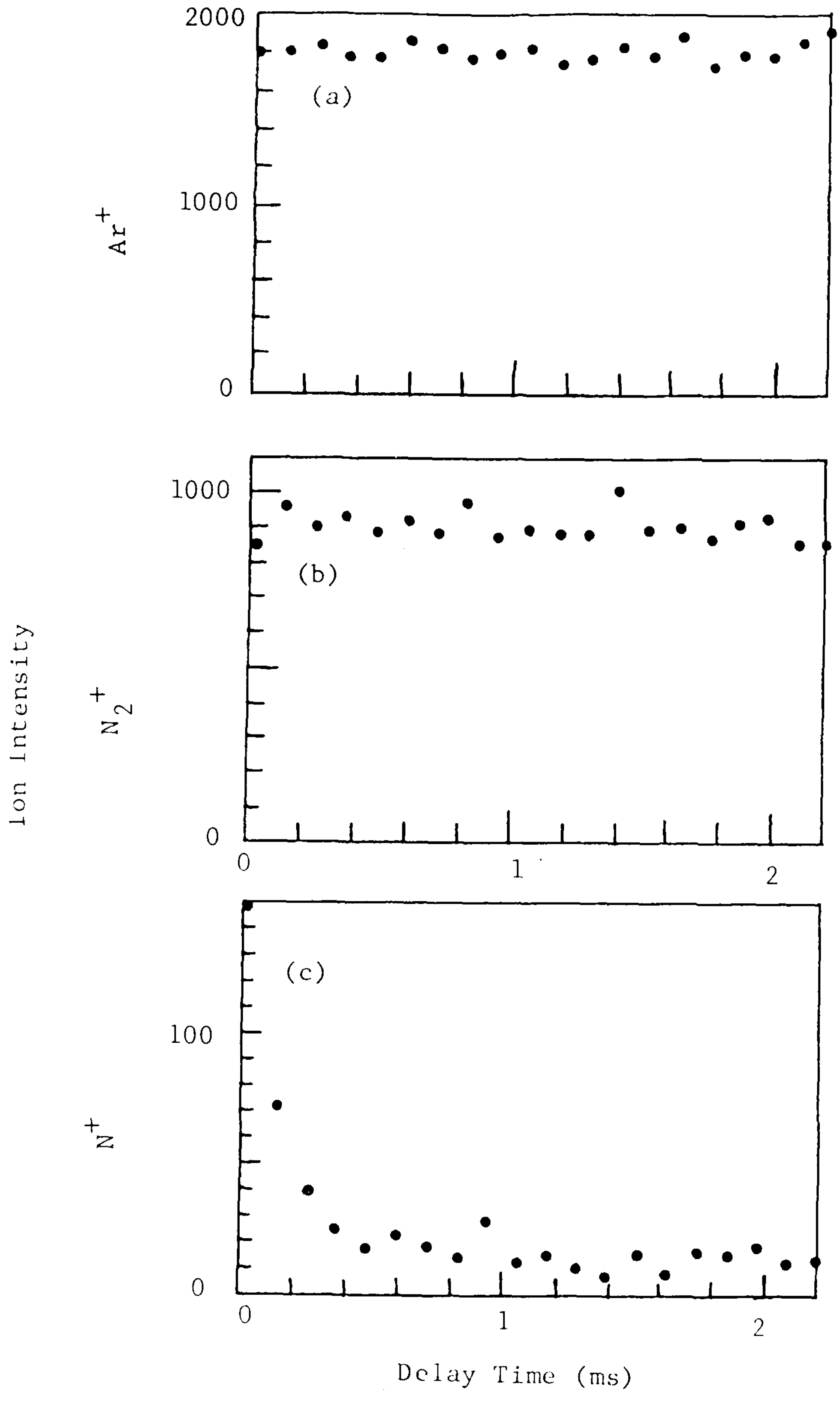

Fig. 2. Laser-enhanced ion production from electron excitation of Ar and N_2 as a function of the delay time with respect to laser pulse.

laser (193 nm) was used. No laser enhancements were detected for the Ar^+ and N_2^+ ion signals produced by electron excitation of Ar and N_2 as shown in Figs. 2(a) and 2(b), respectively. For the N^+ ion production, a laser-enhanced signal was observed right after laser irradiation. The laser-enhanced N^+ production was further investigated as described below.

C. Laser-Enhanced N^+ Production from Electron Excitation of N_2

The enhancement of the N^+ production from electron excitation of N_2 by ArF laser photons was further examined in more detail. The laser-enhanced N^+ signals were measured with a gate period of 5 μs, and the results are shown in Fig. 3, where the laser pulse was at t=0. In the first 10 μs, the signal was interfered by the noise generated by the laser discharge. The ion signal is practically zero in the first 50 μs, which represents the time of flight of the N^+ ions from the laser-electron-molecule interaction region to the ion detector, for which the distance is about 43 cm. This time of flight is consistent with the value calculated from the ion velocity (determined by the ion accelerated energy) and the flight distance. The ion signal lasted about 100 μs, which represents the extraction time of ions from the interaction region. The N^+ ions carry kinetic energy from the electron and/or laser dissociation of N_2 or N_2^+, and move in all directions; thus, it takes a long time to completely extract all ions to the quadrupole.

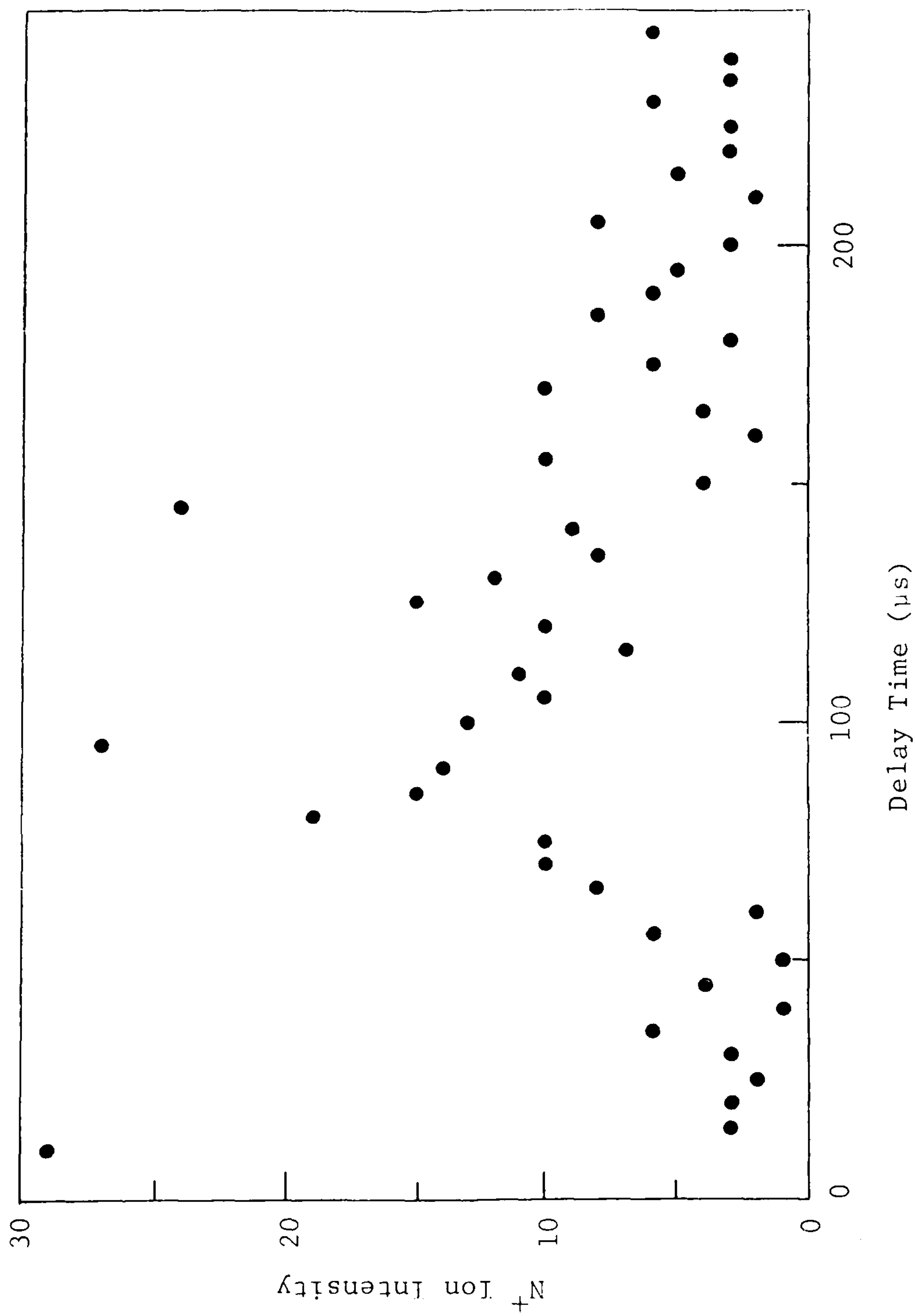

Fig. 3. Laser-enhanced N^+ ion intensity as a function of the delay time with respect to laser pulse.

In order to obtain the laser-enhanced signals, two counters A and B are alternately used to count the pulses. Both have the same gate widths, but different delay times with respect to laser pulses. The pulses counted by A include the continuous background and the laser-enhanced signal; and the pulses counted by B include the continuous background only. The laser-enhanced signal is determined by the difference of counters A and B.

The N^+ ion signals from counters A and B were observed as a function of electron energy as shown in Fig. 4. The signal of counter A is persistently larger than that of counter B. The differences of these two counters are shown in Fig. 5 where the laser-enhanced ion signal starts from 17 eV. Since the electron beam energy could spread over 1 eV, the energy threshold for the laser-enhanced N^+ signal is really at the electron energy of about 18 eV. This threshold energy is equal to the difference of the dissociative ionization energy of N_2 (24.3 eV) and the laser photon energy (6.4 eV). This result indicates that the enhancement is caused by a dissociative ionization process that requires a stepwise excitation of one electron and one photon.

The stepwise excitation could take place either first by electron excitation of N_2 and then by laser excitation, or vise versa. N_2 could be first excited into the N_2^+ (X and A) states, and then dissociated by a laser photon to produce N^+. Since the Franck-Condon factor and transition probability for the ionization process are high, this stepwise excitation is likely the major channel responsible for the observed N^+ ions. The

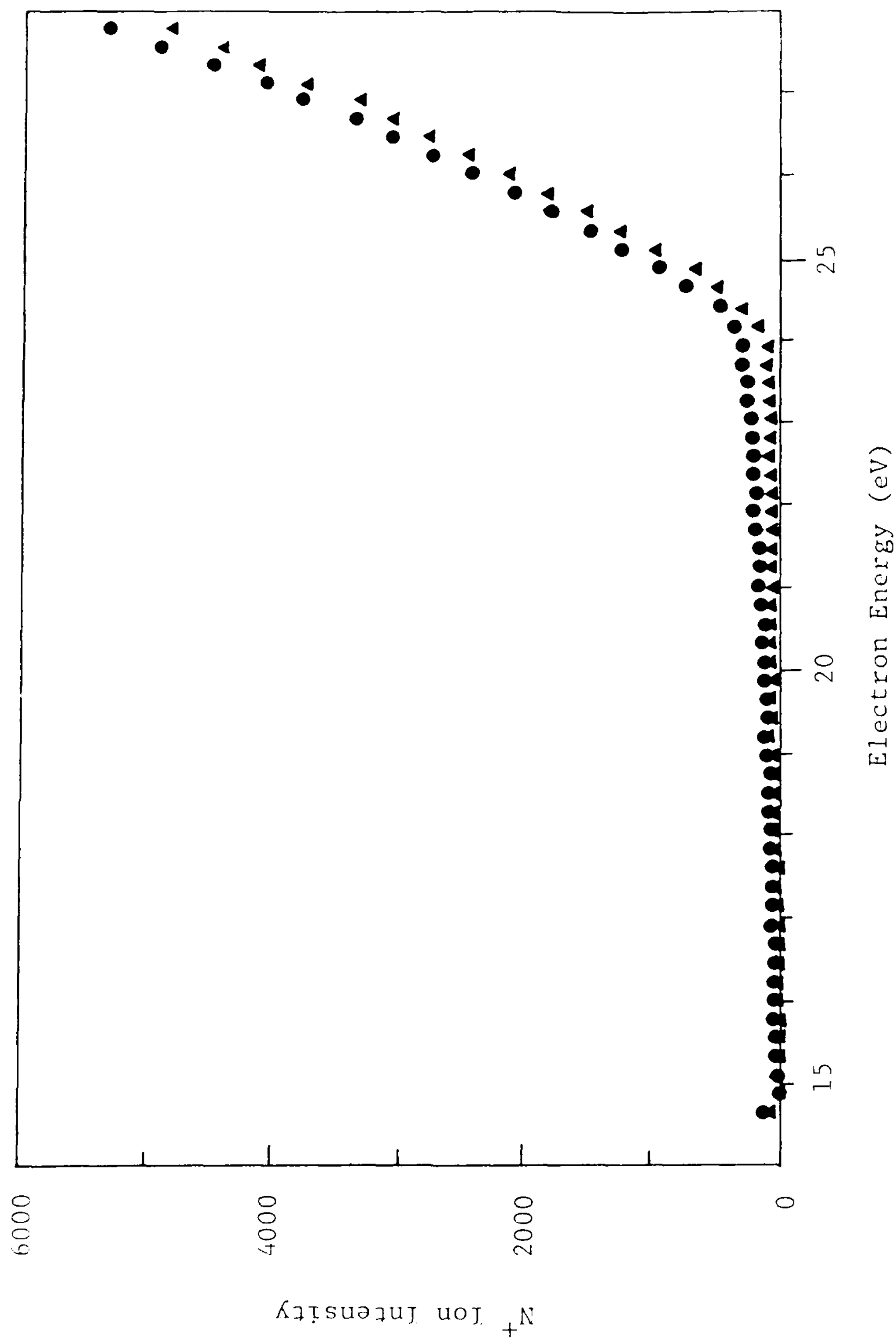

Fig. 4. Production of N^+ ions from electron excitation of N_2. The data indicated by (●) include the laser-enhanced signal and the background signal; and those by (▲) include the background signal only.

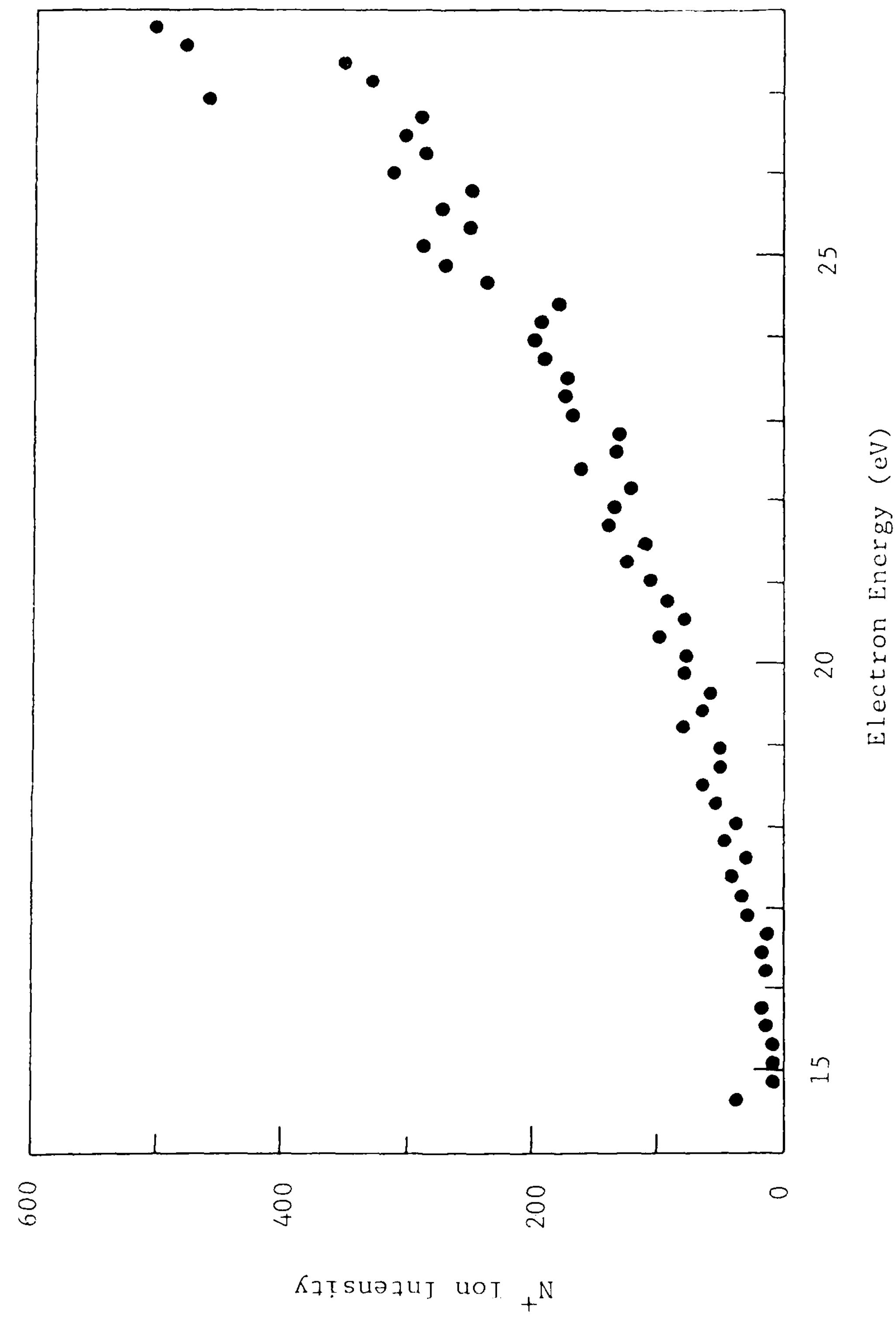

Fig. 5. Laser-enhanced N^+ ion production from electron excitation of N_2 as a function of electron energy.

other channel is first to excite $N_2(X)$ into the $N_2(A^3\Sigma_u^+)$ state by a laser photon and then to produce N^+ by electron excitation. Since both the Franck-Condon factor and the transition probability for the $N_2(X-A)$ transition are small, this channel may have small contribution to the laser-enhanced N^+ ion signal.

It is noted that the signal for the B channel starts at electron energy smaller than the threshold for the dissociative ionization process of N_2 (24.3 eV) as shown in Fig. 4. When the signal of counter B is amplified, the ionization threshold is observed down to 15.6 eV, corresponding to the threshold for the production of $N_2^+(X)$ from electron ionization of N_2. These N^+ ions are likely produced by ionization of N_2^+ by a second electron. We found the N^+ ion intensity produced by electron in the range 16-22 eV depends on the square of electron current. This result suggests that the N^+ ions produced by electron energy < 24.3 eV are due to two-electron excitation process, that is, N_2 is ionized into N_2^+ by an electron of energy > 15.6 eV, and the ion is then dissociated into N^++N by another electron.

The laser-enhanced intensity of N^+ ions was measured as a function of laser power. It is found that the ion intensity is linearly dependent on the laser power as shown in Fig. 6. This result indicates that the N^+ ion is produced by a single photon excitation process. The ions in the $N_2^+(X, v>10$ and $A, v>6)$ excited states, which could be produced by excitation of N_2 with electron energy higher than 18 eV, could be photoionized by a single photon to produce the observed N^+ ions.

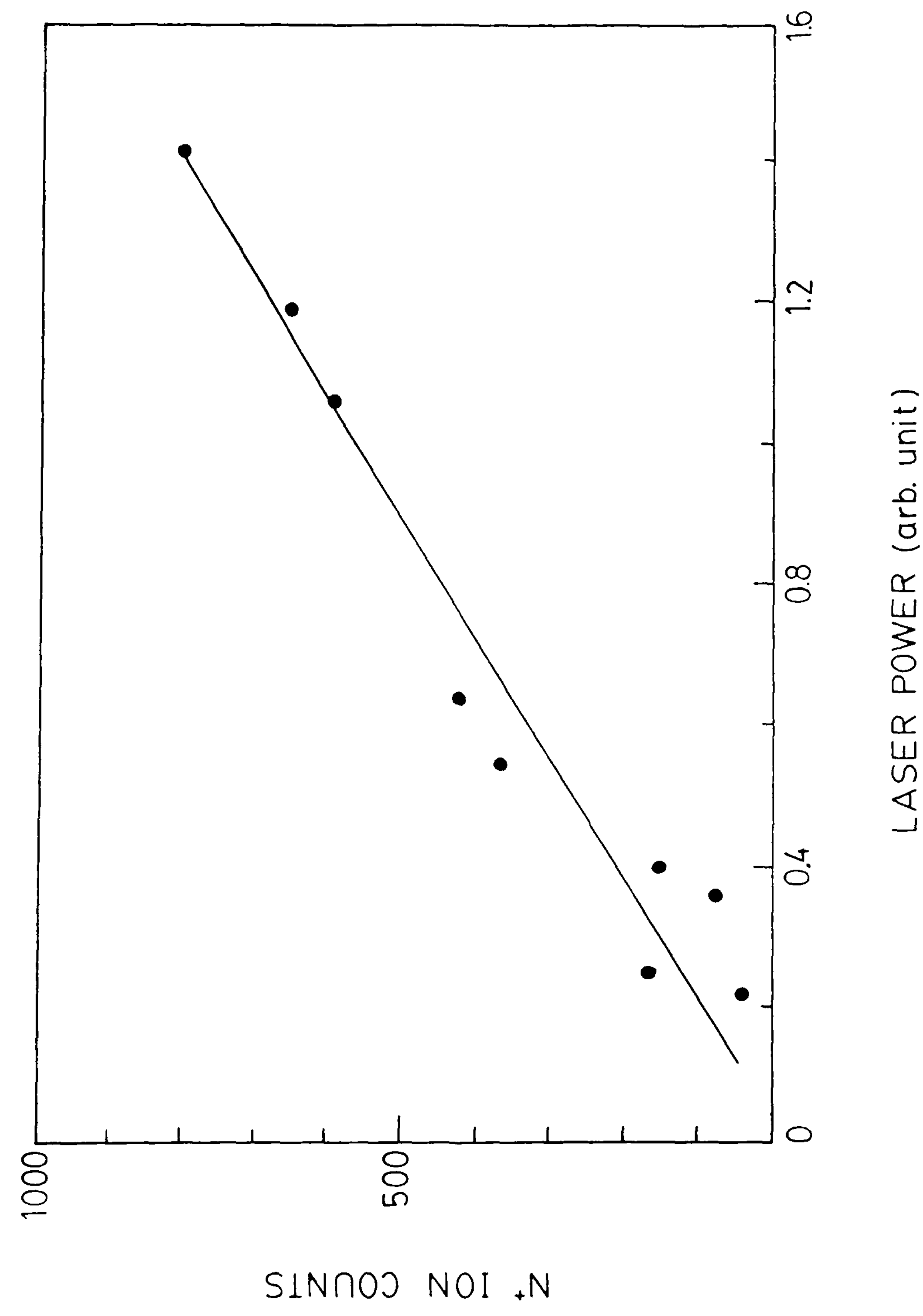

Fig. 6. Laser-enhanced N^+ production from electron excitation of N_2 as a function of laser power.

The dependence of the laser-enhanced N^+ ion intensity on the N_2 pressure was investigated, and the results for an electron energy of 22.6 eV were shown in Fig. 7. Fig. 7(a) shows the signal of counter A that includes both the laser-enhanced signal and the continuous background; Fig. 7(b) shows the signal of counter B for the continuous background; and the laser-enhanced signals are shown in Fig. 7(c) which are the difference of counters A and B. For the continuous background (Fig. 7(b)), the ion intensity is linearly dependent on the gas pressure, indicating that the ion production is not sensitive to quenching. The continuous background ions are produced by electron excitation of N_2^+, which can be in the ground state or any excited states, because the electron energy of 22.6 eV is sufficient to dissociate any N_2^+ into N^++N. On the other hand, the laser-enhanced ion signals are saturated at pressures higher than $2x10^{-7}$ mbar as shown in Fig. 7(a) and 7(c). The laser-enhanced N^+ ions are presumably produced by laser ionization of the excited N_2^+ ions, which are subject to fast quenching by the gas pressure. Once these excited states are quenched to the low vibrational levels of N_2^+(X, v<10 and A, v<6), the laser photon is not energetically possible to dissociate it into N^++N. Thus, the laser-enhanced ion production is sensitive to the gas quenching as shown in Fig. 7(c).

In summary, our experimental observations indicate that the laser-enhanced N^+ ion production form electron excitation of N_2 is likely due to the process that N_2 is first ionized by an

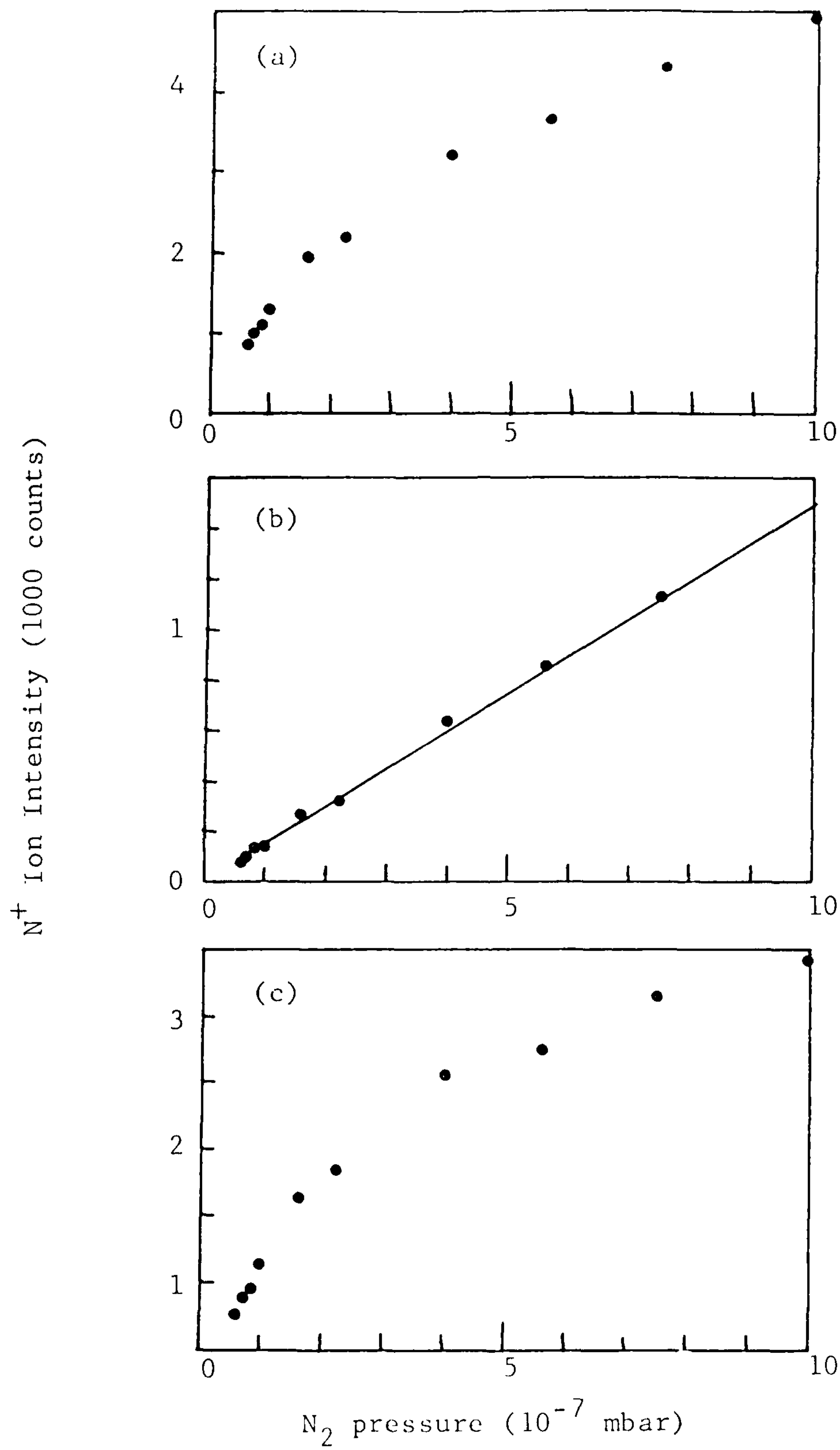

Fig. 7. N^+ ion production from electron excitation of N_2. (a) the sum of the laser-enhanced signal and the background; (b) the background signal; and (c) the laser-enhanced signal.

electron and the ion is then dissociated by a laser photon to produce $N^+ + N$.

D. Laser-Enhanced Ion Production from Electron Excitation of CH_3OH

After the laser-enhanced ionization process of N_2 was reasonably understood, we proceeded to study CH_3OH. CH_3OH could be dissociated by laser photons to produce CH_3 and OH radicals. The laser-enhanced ion signals could be used to derive the electron-impact ionization and electron-attachment cross sections of these radicals. Recently, laser-induced current switching was observed in the discharge media containing CH_3Cl and CH_3Br, which could be useful for the development of gas discharge switches. These observations were reported in the SPIE SDIO Innovative Technology Conference which is attached in this Report as Appendix A. CH_3 is expected to be abundant in these discharge media. The cross sections of various electron excitation processes are needed for understanding the transient discharge phenomena. In addition, CH_3 is an important radical used in the deposition of diamond film, the electron excitation cross sections are needed for modelling the chemical processes of plasma that produces a high concentration of CH_3. The photodissociation process of CH_3Cl, which could be another useful source for the production of CH_3, was also studied in this reporting period. The result is described in more detail in the paper attached as Appendix B.

The mass spectrum for the positive ions produced from electron excitation of CH_3OH at an electron energy of 17.6 eV is

shown in Fig. 8(a). The absolute cross sections for the production of various positive ions at an electron energy of 100 eV have been measured in this research program at the Jet Propulsion Laboratory. The results are included in this Report attached as Appendix C. These absolute cross sections will be used for calibrating the absolute cross sections of radicals. When CH_3OH was irradiated by 193 nm excimer laser, additional ion signals were observed as shown in Fig. 8(b). This mass spectrum was taken by the difference of counters A and B, and it was accumulated over five scans in comparison with the data shown in Fig. 8(a) that was taken by one scan. Fig. 8(b) shown that every ion production is enhanced by laser irradiation, but the enhancement factor is different for each ion species.

The laser-enhanced ion production can be caused by different laser processes: (1) CH_3OH is first dissociated into fragments by laser photons and then ionized by electrons; (2) CH_3OH is first excited by laser photons and then ionized by electrons; and (3) the ions of CH_3OH^+, CH_3^+, CHO^+, etc., produced by electron excitation are dissociated by laser photons. The ion signal produced by multiphoton ionization process (with laser irradiation but no electron beam) is more than two orders of magnitude smaller than the laser-enhanced signal; thus, the contribution of the multiphoton ionization process is neglected. Our main goal of this experiment is to measure the electron excitation cross sections of radicals that could be determined from the laser-enhanced signals. However, the contribution of

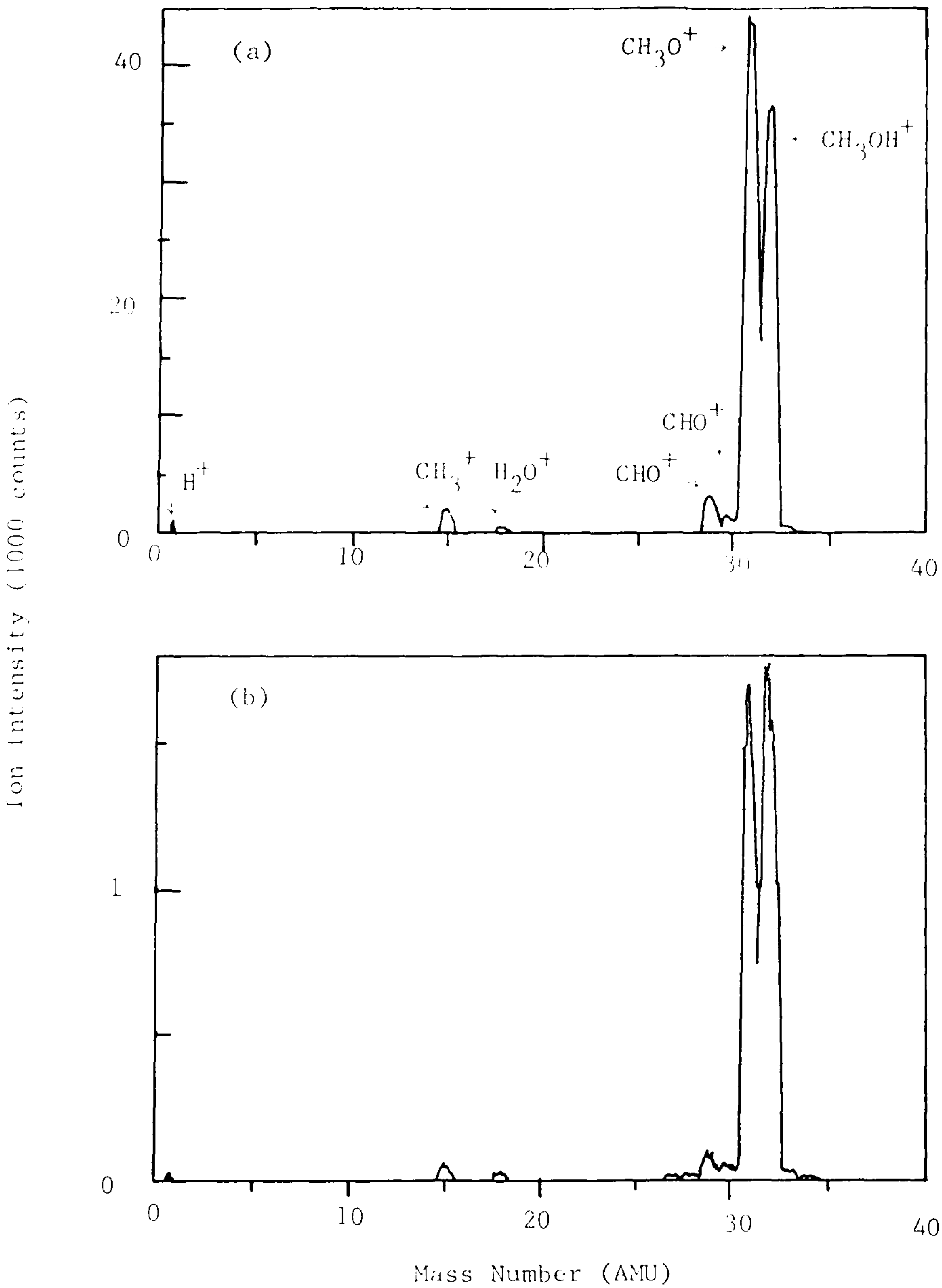

Fig. 8. Mass spectra of (a) electron ionization of CH_3OH and (b) laser-enhanced ion production.

each process needs to be well established, before this goal can be achieved.

For a further study of the laser-enhanced ionization mechanism of CH_3OH, the laser-enhanced signals of CH_3^+ (which was selected by the mass spectrometer) were studied as a function of electron energy, laser power, gas pressure, and electron beam current. The CH_3^+ ion signals from electron excitation of CH_3OH with (counter A) and without (counter B) laser irradiation are shown in Fig. 9(a). The difference between these two counters are shown in Fig. 9(b). The laser-enhanced ion signals increase with electron energy at a threshold energy of 15 eV. The enhanced signal is linearly dependent on the laser power as shown in Fig. 10 as well as on the electron beam current as shown in Fig. 11. The enhanced signal is saturated at pressures higher than 10^{-7} mbar as shown in Fig. 12, where the signals of counter A are shown in (a), counter B in (b), and the difference of A-B in (c). The excitation process of CH_3OH is very complicated, because it can occur through many dissociation channels. The present data are not sufficient to determine the enhancement mechanism uniquely. We will continue this study in the next funding period.

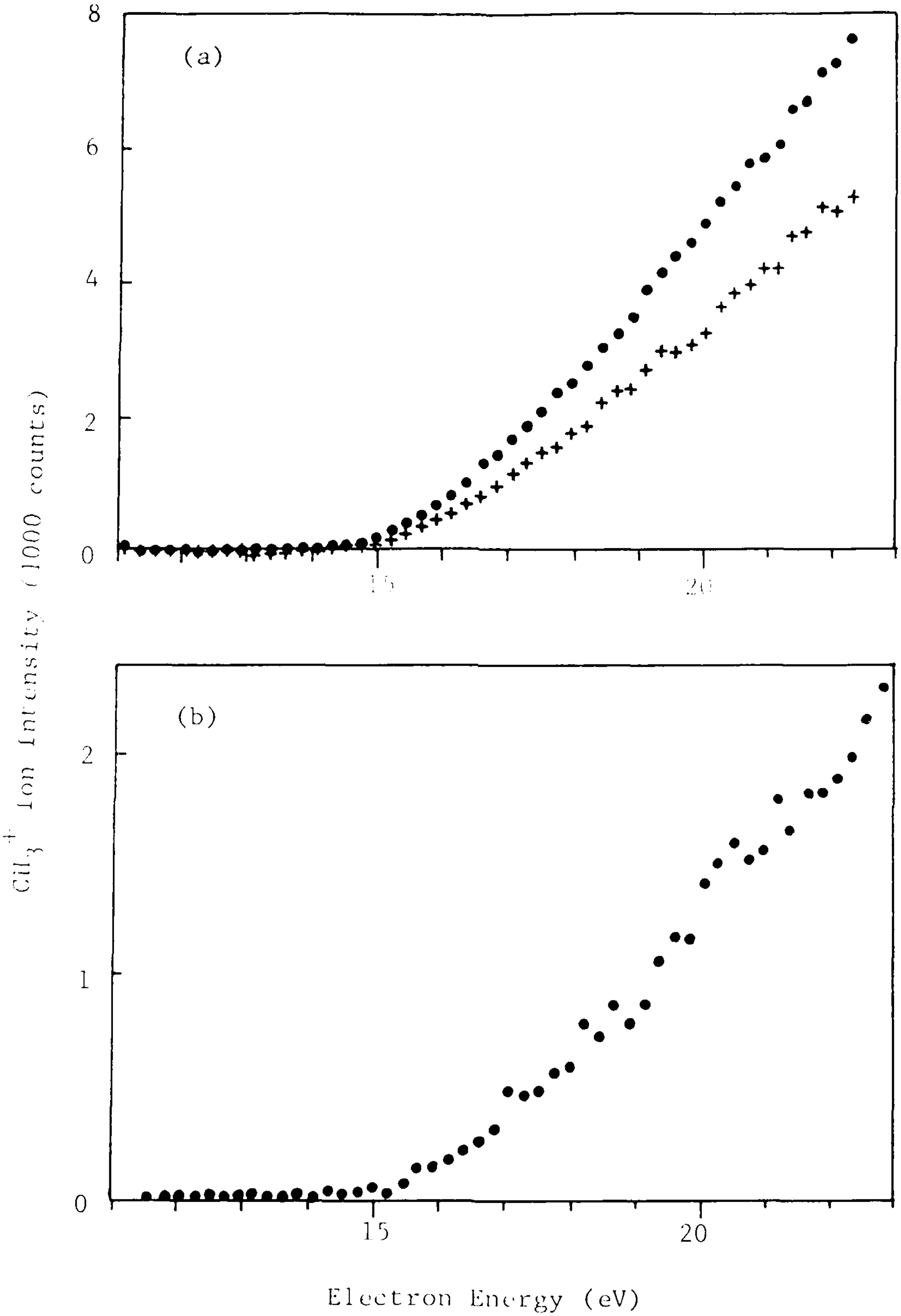

Fig. 9. (a) CH_3^+ ion production from electron excitation of CH_3OH as a function of electron energy. (●) is the sum of the laser-enhanced signal and the background and (+) is the background only. (b) The laser-enhanced CH_3^+ ion signal.

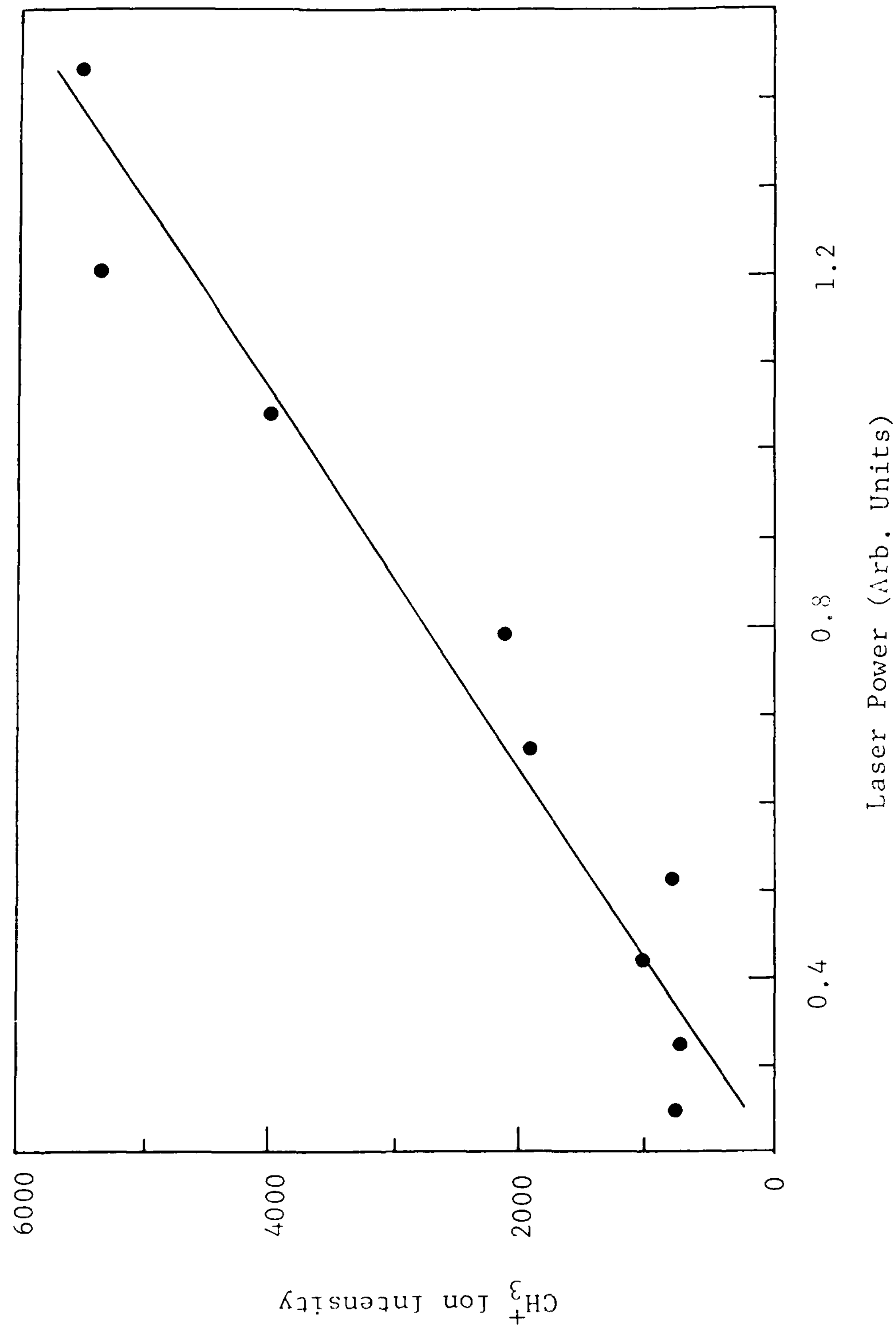

Fig. 10. Laser-enhanced CH_3^+ production from electron excitation of CH_3OH as a function of laser power.

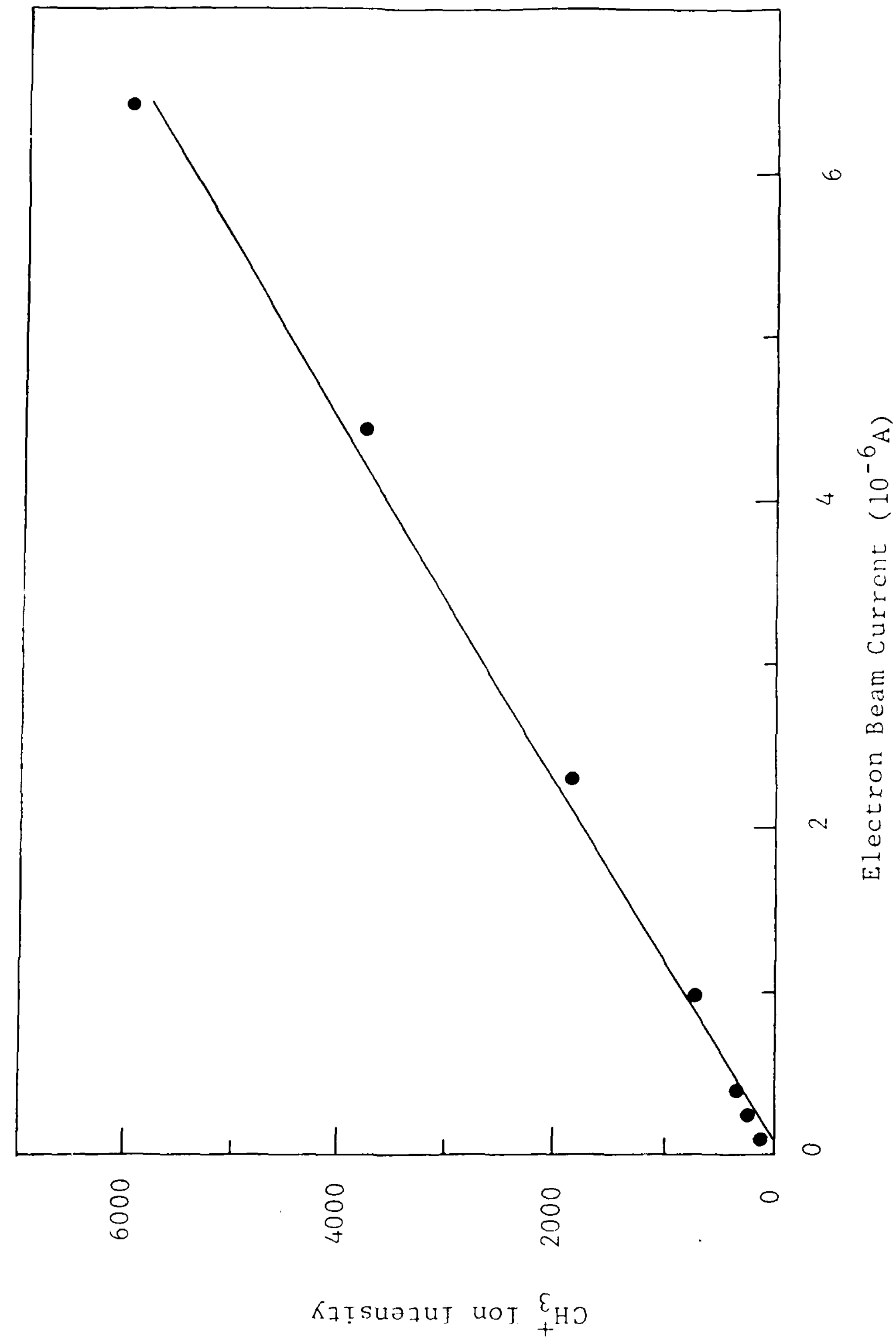

Fig. 11. Laser-enhanced CH_3^+ ion intensity as a function of electron beam current.

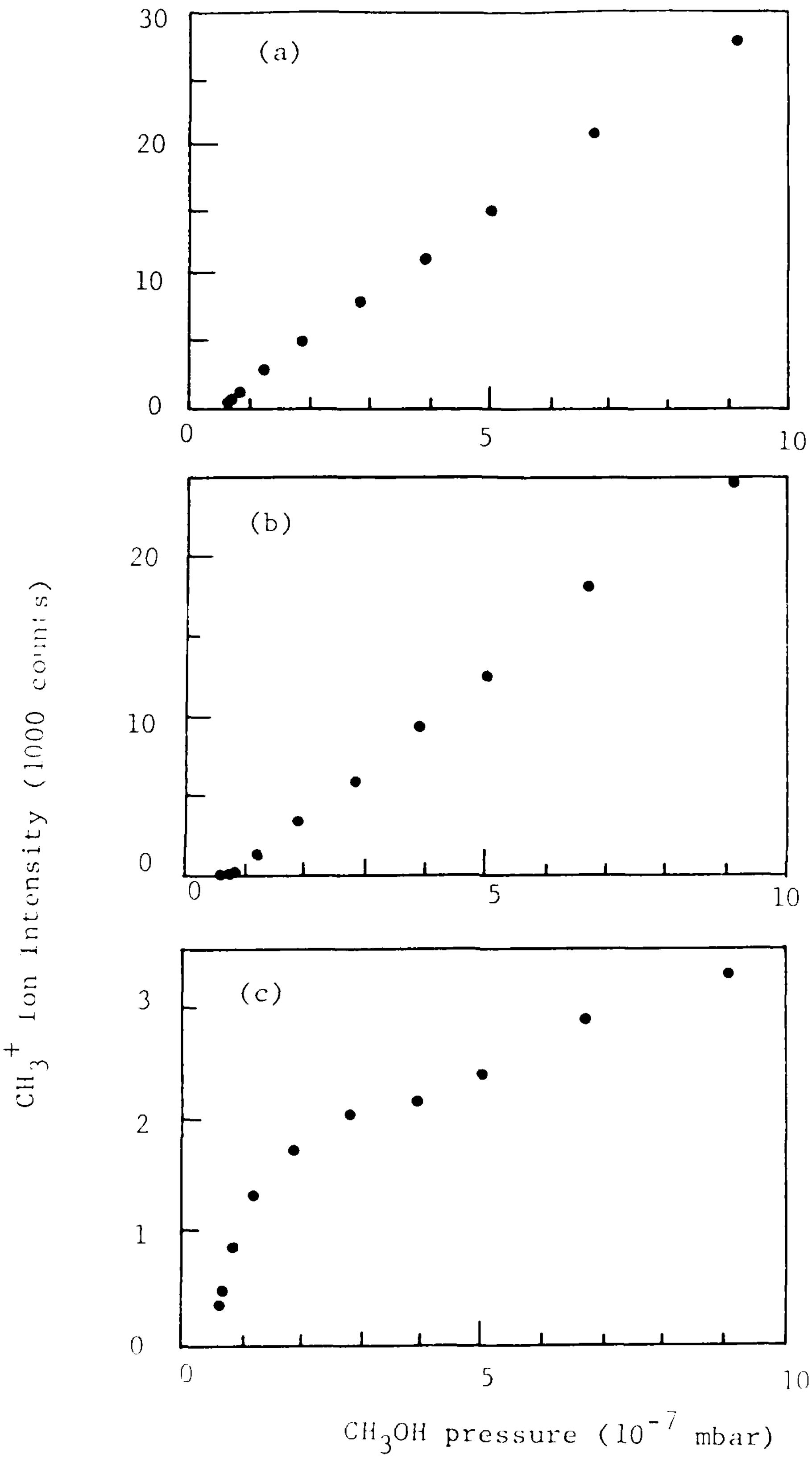

Fig. 12. CH_3^+ production from electron excitation of CH_3OH as a function of gas pressure. (a) the sum of the laser-enhanced signal and the background; (b) the background only; and (c) the laser-enhanced signal (difference of (a) and (b)).

III. Research Plan for the Next Funding Period

More data for the laser-enhanced ion production from electron excitation of CH_3OH will be taken for the understanding of the mechanism that causes the enhancement. The laser enhancement for the production of CH_3OH^+, CH_3^+, CH_2O^+, CH^+, and OH^+ will be measured as a function of electron energy, laser power, gas pressure, and electron beam current. Once the mechanism is well understood, we will proceed to determine the absolute electron-impact ionization cross sections of radicals.

We also plan to study the laser-enhanced ion production using other laser wavelengths, for example, F_2 laser at 157 nm and KrF laser at 248 nm. We will extend the study to other molecules that contain the CH_3 radical, for example, CH_3Cl, $(CH_3)_2O$, and $(CH_3)_2CO$. These proposed study will provide additional information to support the CH_3 data obtained from electron excitation of CH_3OH.

Appendix A

"Laser-Induced Current Switching in Gaseous Discharge"

Long C. Lee, Wen C. Wang, and Dong P. Wang

Presented at the IS&T Technical Conferences, SPIE O-E/LASE '88, 10-17 January, 1988, Los Angeles, California

Laser-Induced Current Switching in Gaseous Discharge

Long C. Lee, Wen C. Wang and Dong P. Wang

Department of Electrical and Computer Engineering
San Diego State University, San Diego, California 92182

ABSTRACT

Current increase induced by laser photodetachment of negative ions and current decrease due to laser modification of gas property were observed. This current switching could be applied for the development of discharge switches. Basic data (such as electron drift velocity, photodetachment cross section, electron attachment rate, and electron-impact ionization cross section) are being measured for such applications.

1. INTRODUCTION

Discharge current will increase when negative ions in a discharge medium are photodetached to produce conduction electrons, because electron in a gas medium has a drift velocity faster than negative ion by a factor of 10^3-10^4. Enhancement of discharge current by photodetachment of halogen negative ions (F^-, Cl^-, Br^- and I^-) in discharge media containing halogen compounds was recently observed in our experiment. The decrease of discharge current due to the change of gas property by laser excitation was also observed. This transient phenomenon has a potential application for the development of gaseous discharge switches. Basic data needed for such application are being measured in our experiment and presented in this conference.

2. EXPERIMENT

The experimental apparatus for the observation of laser-induced current switching and the measurements of basic data (electron drift velocity, electron attachment rate constant of electronegative gas and photodetachment cross section of negative ion) was described in a previous paper.[1] In breif, point-to-plane electrodes were set inside a gas cell of 6" OD six-way cross to produce DC discharge current. The cathode was a steel wire, and the anode was a stainless steel plate. A negative high voltage was applied to the cathode, and the discharge current was measured by the voltage across a resistor that connected the anode to ground. An excimer laser was used to induce the current switching. For the measurements of electron drift velocity and electron attachment rate constant, two parallel uncoated stainless steel plateds were used as electrodes. Electrons were produced by irradiation of cathode with excimer laser photons. The number of electrons was monitored by conduction current induced by electron motion between electrodes.

The experimental apparatus for the measurements of electron-impact-ionization and electron attachment cross sections of molecules and radicals is shown in Fig. 1. The radicals are produced by photodissociation of molecules by vacuum ultraviolet laser photons. The radicals are impacted by electron beam that has an energy resolution of about 0.5 eV in the energy range of 0-300 eV. The positive and negative ions produced from electron impact excitation of molecules and radicals are analyzed and detected by a mass spectrometer.

3. RESULTS

3.1. Switching of Discharge Current

When a discharge medium was irraciated by an excimer laser pulse, the discharge current increased initially and then recovered after a few μs. This current increase is attributed to electrons released from photodetachment of negative ions by laser photons. The transient current pulses usually recover to the DC level; but for some instances, the transient pulses decrease below the DC level as shown in Figs. 2 (b) and (c). This decrease is due to the modification of gas attachment rate by laser photons.

The observed current switching can be applied to the design of discharge switches. Electron transport parameters are needed for the assessment of this applicability, which are described below.

3.2. Photodetachment cross sections of Negative Ions

The photodetachment cross section is needed to determine the laser power required to totally photodetach electrons from negative ions. This parameter can be measured from the increase of transient current as a function of laser power. The photodetachment cross

sections[2] of F^-, Cl^-, Br^- and I^- at 193 and 248 nm measured in the discharge media of various halogen compounds in N_2 are listed in Table 1.

Table 1. Photodetachment cross sections of Halogen Negative Ions.

	193 nm (10^{-18} cm^2)	248 nm (10^{-18} cm^2)
F^-	7.5	6
Cl^-	25	10
Br^-	32	15
I^-	70	30

3.3. Electron Drift Velocity

The magnitude of electron conduction current depends linearly on the electron drift velocity. The electron drift velocity could be affected by the composition of a gas mixture. For example, when a trace of CH_3Br is added to Ar, the electron drift velocity[3] increases greatly as shown in Fig. 3.

3.4. Electron Attachment Rate Constant

The electron attachment rate constant is an essential parameter for determining the formation rate of negative ion as well as the opening time of a discharge switch. The electron drift attachment rate constants of HBr and CH_3Br are shown in Figs. 4 and 5.

3.5. Electron Attachment to Radicals in Discharge Media

In an electrical discharge medium, a large fraction of molecules dissociates into radicals. For example, the CH_3 radical is expected to be abundant in the discharge medium of trace CH_3Br in N_2 or Ar, because CH_3Br will be dissociated into CH_3 + Br by electron impact. Thus the rate constants and cross sections of electron attachment and electron-impact ionization of radicals are important in studying the transient phenomena of electrical discharges. These data are, however, not available in the literature. These data of radicals are currently under study in our laboratory. The radicals (such as CH_3 and OH) will be produced by photodissociation of molecules (CH_3Cl, CH_3Br, CH_3OH and H_2O) by excimer laser photons. Electron-impact-ionization and electron attachment processes such as,

$$CH_3 + e \rightarrow CH_3^+ + 2e$$
$$\rightarrow CH_2^+ + H + 2e$$
$$\rightarrow CH^+ + 2H + 2e$$
$$\rightarrow C^+ + 3H + 2e$$
$$\rightarrow CH_2^- + H$$
$$\rightarrow CH^- + 2H$$
$$\rightarrow C^- + 3H$$
$$\rightarrow CH_2 + H^-$$

are being invesitgated.

4. APPLICATION FOR DISCHARGE SWITCHES

The current switching and the basic data presented above could be used to design discharge switches. As an illustration, discharge medium of trace HBr and CH_3Br in Ar (or N_2) is considered for such application. Br^- could be totally photodetached by an ArF laser pulse energy of 0.1 J/cm^2 as calculated from the photodetachment cross section listed in Table 1. At E/N= 1 Td (10^{-17} V cm^2), the drift velocity[4] of a negative ion in Ar is about 10^3 cm/s, and the electron drift velocity is about 10^6 cm/s (see Fig. 3). Thus, the transient current due to laser-detachment of Br^- could be 10^3 times more than the DC discharge current and the switching power. As calculated from the electron attachment constant shown in Fig. 4, the recovery time for the transient pulse could be less than 1 μs, if 0.3 torr of HBr is mixed in the discharge medium. This example demonstrates that the gas mixture of trace HBr and CH_3Br in Ar or N_2 could be used for the switching of high electrical energy.

5. ACKNOWLEGEMENT

This presentation is based on the work sponsored by the AFOSR and by the SDIO/IST managed by ONR.

6. REFERENCES

1. W.C. Wang and L. C. Lee, "Laser-Induced Current Switching Observed in Discharge Media of CF_2Cl_2-N_2 and CH_3Cl-N_2," IEEE Trans. Plasma Sci. PS-15,460-466, (1987).

2. W. C. Wang and L. C. Lee, "Photodetachment Cross Sections of Negative Halogen Ions in Discharge Media," J. Phys. D: Appl. Phys. Submitted for publication (1987).

3. W. C. Wang and L. C. Lee, "Electron Attachment Rate Constants of HBr, CH_3Br, and C_2H_5Br in N_2 and Ar," Submitted to J. Appl. Phys. in press (1987).

4. H. W. Ellis, R. Y. Pai, E. W. McDanial, E. A. Mason, L. A. Viehland, Atomic Data & Nuclear Tables, 17, 177-210 (1976).

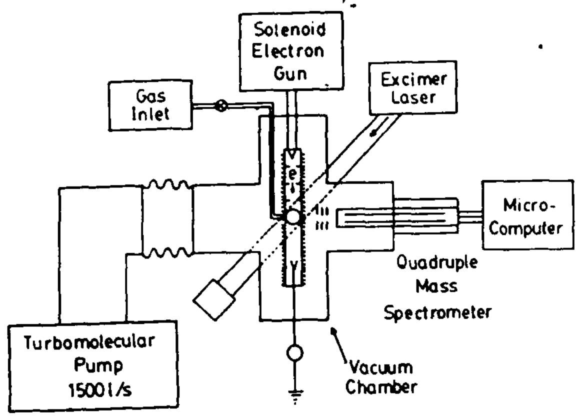

Fig. 1 Experimental setup for measuring electron attachment and electron impact ionization cross sections of radicals

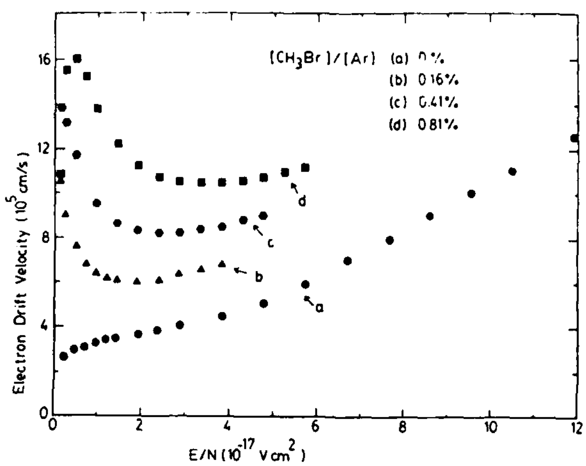

Fig. 3 Drift velocities of electrons in the gas mixture of CH_3Br in Ar as a function of the CH_3Br concentration

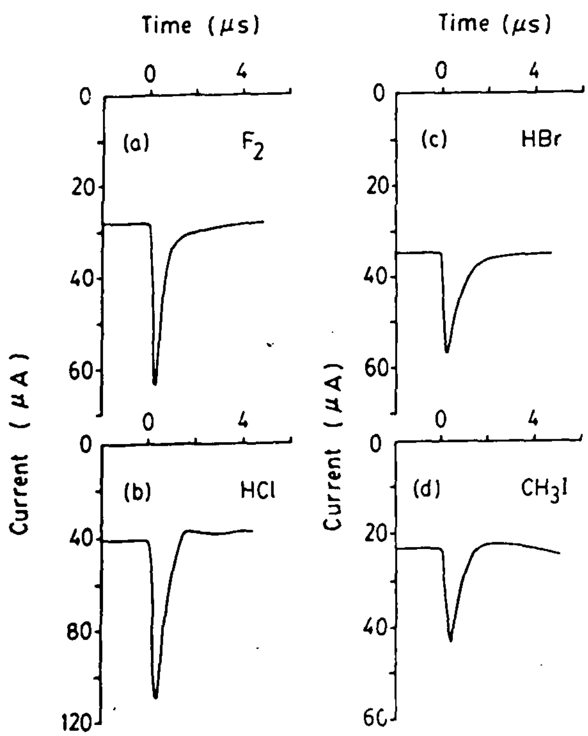

Fig. 2 Laser-induced current switching observed in discharge media of trace halogen compounds in N_2

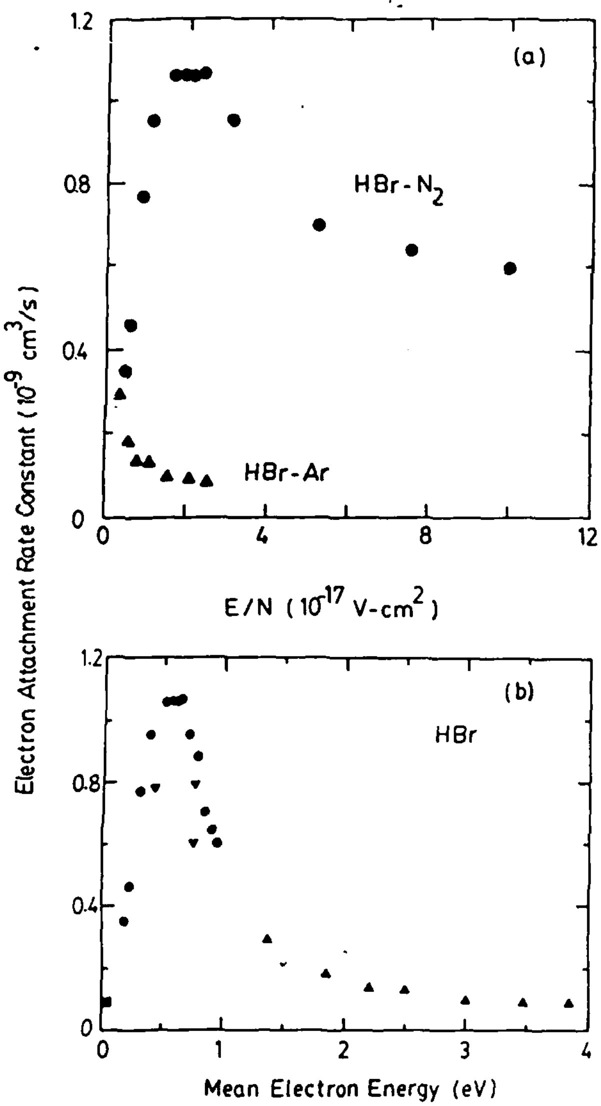

Fig. 4 Electron attachment rate constant of HBr as a function of (a) E/N and (b) mean electron energy

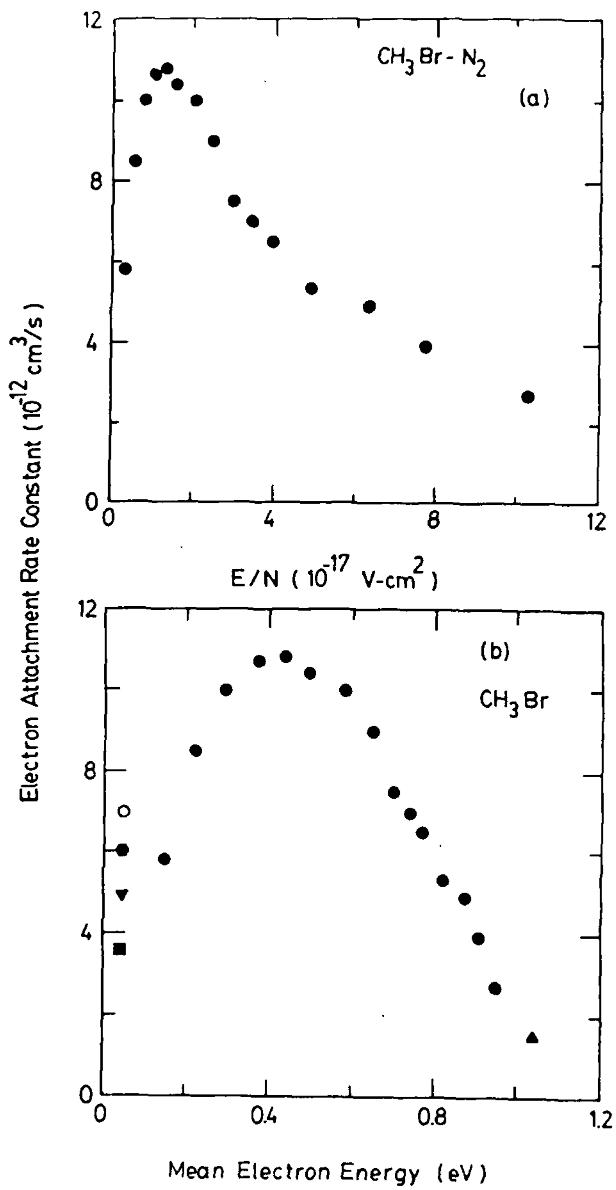

Fig. 5 Electron attachment rate constant of CH_3Br as a function of (a) E/N and (b) mean electron energy

Appendix B

"Fluorescence Yields from Photodissociative Excitation of Chloromethanes by Vacuum Ultraviolet Radiation"

L. C. Lee and M. Suto

Chemical Physics 114, 423 (1987)

Chemical Physics 114 (1987) 423–429
North-Holland, Amsterdam

FLUORESCENCE YIELDS FROM PHOTODISSOCIATIVE EXCITATION OF CHLOROMETHANES BY VACUUM ULTRAVIOLET RADIATION

L.C. LEE [1] and Masako SUTO

Department of Electrical and Computer Engineering, San Diego State University, San Diego, CA 92182, USA

Received 28 January 1987

The photoabsorption and fluorescence cross sections of chloromethanes were measured in the 105–220 nm region using synchrotron radiation as a light source. The fluorescence threshold for CCl_4 is at 152 nm with a maximum yield of 3% at 113 nm. The fluorescence results from the $CCl_2(\tilde{A}-\tilde{X})$ system. For $CHCl_3$, the fluorescence threshold is at 155 nm with a maximum yield of 0.6% at 110 nm. For CH_2Cl_2, the threshold is at 137 nm with a maximum yield of 0.35% at 107 nm. The fluorescence yield of CH_3Cl is very small with an upper limit of 0.02%. The photodissociation processes are discussed in accord with the fluorescence data observed. Vibrational structures in $CHCl_3$ and CH_3Cl_2 are observed and classified into progressions.

1. Introduction

Fluorescence from vacuum ultraviolet (VUV) photolysis of CCl_4 was recently observed and identified to be the $CCl_2(\tilde{A}\,^1B_1 \rightarrow \tilde{X}\,^1A_1)$ system [1]. The fluorescence excitation spectrum was reported [1], but the fluorescence cross section and quantum yield were not measured. It is of interest to measure the quantitative data, because they are important for understanding photodissociation processes as well as for practical applications. For example, the production yields of atomic Cl from photolysis of chlorine compounds are of interest in the study of atmospheric and intersteller chemistry and in the chemical etching of semiconductor materials. Photolyses of chloromethanes could be sources of CH_x ($x = 1$–3) radicals.

The absolute cross sections for photoabsorption and fluorescence of chloromethanes (CCl_4, $CHCl_3$, CH_2Cl_2 and CH_3Cl) were measured using synchrotron radiation as a light source. The absorption cross sections are used to compare, with previous values [1–5] that are somewhat controversal [1]. The quantitative fluorescence cross sections and quantum yields reported here are new results.

[1] Also at: Department of Chemistry, San Diego State University, San Diego, CA 92182, USA.

2. Experimental

The experimental arrangement has been described in previous papers [6,7]. In brief, synchrotron radiation produced from the electron storage ring at the University of Wisconsin was dispersed by a 1 m Seya vacuum monochromator. The absorption cross section was measured by the attenuation of light source by molecules in a gas cell of 39.2 cm path length. The experimental uncertainty for the absorption cross section is estimated to be within 10% of the given value. The VUV light intensity was measured by a combination of sodium salicylate coated on a window and a photomultiplier tube (PMT). The fluorescence was observed in a direction perpendicular to the light source by a PMT (EMI 9558QB), for which the response was about constant in the 180–400 nm region and then gradually decreased to nearly zero at about 800 nm. The absolute fluorescence cross section was obtained by comparing the fluorescence intensity with the OH(A–X) fluorescence produced from photodissociative excitation of

H_2O, for which the fluorescence cross section is known [6,7]. The PMT response was not corrected in the absolute fluorescence measurement. The fluorescence cross section could be higher than the given value by a factor of two, if the correction for the PMT response is made.

Liquid CCl_4 was supplied by EM Industries with a stated purity of better than 99.9%. Liquid $CHCl_3$ and CH_2Cl_2 were supplied by Fisher Scientific with purities of better than 99.7% and 99.9%, respectively. These liquids were degassed by cooling down to solid with liquid N_2. The samples were repeatedly purified such that the absorption due to possible impurities, such as O_2, was not observed in the absorption spectra. CH_3Cl was supplied by Matheson with a purity of better than 99.5%, and was used in the experiment as delivered.

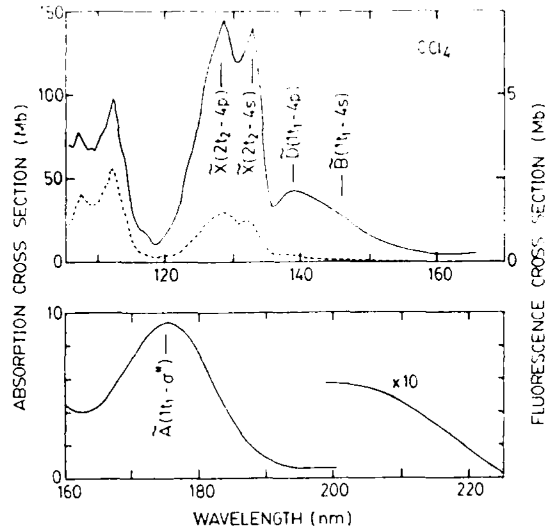

Fig. 1. Photoabsorption (———) and fluorescence (---) cross sections of CCl_4 measured with a monochromator resolution of 0.2 nm.

3. Results and discussion

3.1. CCl_4

The absorption cross section of CCl_4 in the 105–220 nm region is shown in fig. 1, which was measured with a monochromator resolution of 0.2 nm. The absorption bands have been assigned to Rydberg states as discussed by several investigators [3,8], and the assignment given by Robin [8] is indicated in fig. 1. The discrepancy between the earlier absorption data has been pointed out by Ibuki et al. [1]. The current result agrees within experimental uncertainty with the data of Russell et al. [3] in the 110–200 nm region, but it is higher than the data of Ibuki et al. by about 40% in the 110–135 nm region.

The cross section for the production of fluorescence from photodissociative excitation of CCl_4 is shown in fig. 1. The fluorescence was observed simultaneously with the absorption measurement. The fluorescence has been attributed to the $CCl_2(\tilde{A}-\tilde{X})$ system [1]. The structure shown in the fluorescence cross section is very similar to that of the absorption cross section.

The fluorescence yield, which is defined as the ratio of fluorescence cross section to absorption cross section, is shown in fig. 2a. The fluorescence yield starts at 152 nm, increases to a plateau of about 1% at 130 nm, and then reaches a maximum of about 3% at 113 nm.

The fluorescence yield is a measure of the interaction strength between the initial excited state and the repulsive state that produces the emitting species. The vertical energy of the repulsive state

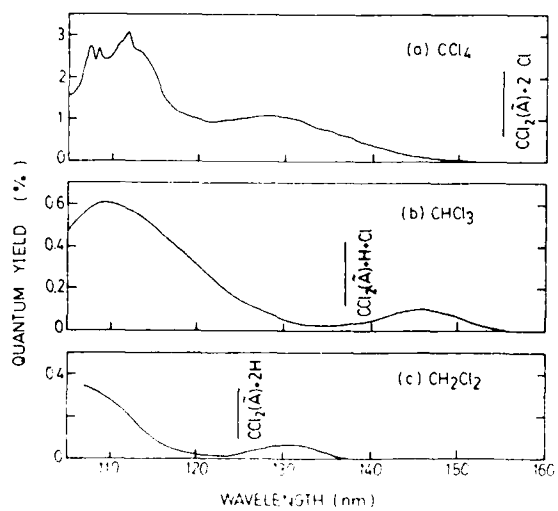

Fig. 2. Fluorescence quantum yields of (a) CCl_4, (b) $CHCl_3$, and (c) CH_2Cl_2. The calculated thresholds for the dissociation processes that produce CCl_2 $(\tilde{A}-\tilde{X})$ fluorescence are indicated.

can be determined from the wavelength at the maximum fluorescence yield. The first repulsive state, which has a maximum fluorescence yield at 128 nm (vertical energy of 9.7 eV), may dissociate into $CCl_2(\tilde{A}) + Cl_2$. The threshold wavelength for this process is at 224 nm. The second repulsive state, which has a maximum fluorescence yield at 1. nm (vertical energy of 11.0 eV), likely dissociates into $CCl_2(\tilde{A}) + 2Cl$. The threshold for this process is at 155 nm. The threshold wavelengths are calculated using the heats of formation for CCl_4, CCl_2, and Cl of −22.42, 56.7, and 28.587 kcal/mol, respectively [9,10], the dissociation energy of $D_0(Cl-Cl) = 2.479$ eV [11], and the excitation energy for the $CCl_2(\tilde{A}\ ^1B_1(0,0,0) \leftarrow \tilde{X}\ ^1A_1(0,0,0))$ transition of 2.1 eV [12].

3.2. $CHCl_3$

3.2.1. Photoabsorption

The photoabsorption cross section of $CHCl_3$ is shown in fig. 3, which was measured with a monochromator resolution of 0.4 nm. The current result is generally higher than the data of Russell et al. [3] by about 25%, and significantly higher than the data of Lucazeau and Sandorfy [2].

The absorption bands of $CHCl_3$ have been previously assigned to Rydberg transitions [3,8], and the assignment given by Robin [8] is indicated in fig. 3. In addition to the broad absorption bands, weak vibrational structures were observed in the absorption spectrum. The absorption spectrum measured with a monochromator resolution of 0.04 nm is shown in fig. 4. The first vibrational progression is superimposed on the 3e → 4p Rydberg transition, indicating that the vibrational progression may be a member of the Rydberg series converging to the ^2E ion state of $CHCl_3$. The absorption spectra for the $\tilde{D}(1a_2 \rightarrow 4p)$ and $\tilde{X}(3e \rightarrow 4p)$ Rydberg transitions are very similar to the photoelectron spectra of the $^2A_2$ and ^2E ion states of $CHCl_3^+$ [13,14]. This similarity further suggests that the first level of the vibrational progression at 136.61 nm likely converges to the threshold of the ^2E ion state which is at 11.6 eV [13,14]. Based on this assumption, the effective quantum number for the Rydberg transition is calculated by the Rydberg formula,

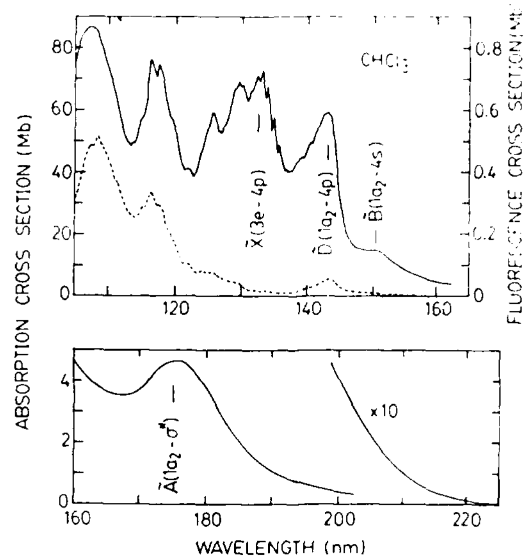

Fig. 3. Photoabsorption (———) and fluorescence (---) cross sections of $CHCl_3$ measured with a monochromator resolution of 0.4 nm.

$$\nu = \nu_0 - 109737/n^{*2}, \tag{1}$$

where $\nu_0 = 93560$ cm^{-1} is the threshold potential energy of the ^2E ion state [13,14]. The effective quantum numbers, wavelengths, wave numbers, and vibrational frequencies for the tentatively as-

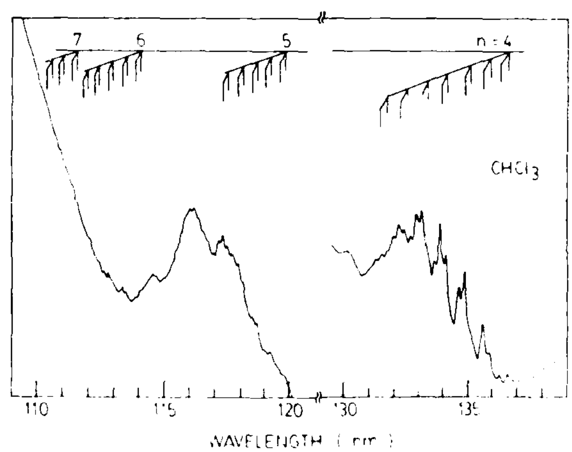

Fig. 4. Photoabsorption spectrum of $CHCl_3$ measured with a monochromator resolution of 0.04 nm. The wavelength positions for the vibrational progressions of tentatively assigned Rydberg series are indicated.

signed vibrational progressions of other Rydberg members are listed in table 1 as well as indicated in fig. 4. The wavelength is calibrated against the known absorption spectra of CH_3Cl [15] and H_2O [16] which were measured in the same experiment. The uncertainty for the wavelength calibration is estimated to be 0.1 nm for the absolute value and 0.02 nm for the relative value.

As listed in table 1, the average frequency for the vibrational progressions is about 410 cm^{-1}. This value is close to the ν_3 frequency (CCl_3 symmetrical deformation mode) of the ground state of $CHCl_3$ (363 cm^{-1}) [17,18]. As shown in fig. 4, each vibrational band has a double peak with a frequency separation of about 120 cm^{-1}.

3.2.2. Fluorescence

The cross section for the production of fluorescence from photodissociative excitation of $CHCl_3$ was simultaneously measured with the absorption cross section. The result is shown in fig. 3. The fluorescence cross section is used to calculate the quantum yield as shown in fig. 2b. The fluorescence yield starts at 155 nm, and then reaches two maxima of 0.1% and 0.6% at 146 and 110 nm, respectively. The first band likely corresponds to a repulsive state (with a vertical energy of 8.5 eV) that dissociates into

$$CHCl_3 \rightarrow CCl_2(\tilde{A}) + HCl. \quad (2)$$

The threshold wavelength for this process is 268 nm, where the heats of formation of -22.019 and -23.49 kcal/mol for HCl and $CHCl_3$ [9,10], respectively, are used for the calculation.

The second fluorescence band likely corresponds to a repulsive state (with a vertical energy of 11.3 eV) that dissociates into

$$CHCl_3 \rightarrow CCl_2(\tilde{A}) + H + Cl. \quad (3)$$

The threshold for this process is 137 nm, where the dissociation energy of $D_0(H-Cl) = 4.434$ eV [11] is used for the calculation. The calculated threshold wavelength coincides very well with the observed threshold as in fig. 2b.

Table 1
The effective quantum numbers, n^* wavelengths, λ, wave numbers, ν, and vibrational frequencies, $^1\Delta\nu$, for the tentatively assigned vibrational progressions of the Rydberg series converging to the ^2E ion state of $CHCl_3^+$

n	n^*	v	λ (nm)	ν (cm^{-1})	$\Delta\nu$ (cm^{-1})
4	2.32	0	136.61	73201	404
		1	135.86	73605	436
		2	135.06	74041	541
		3	134.08	74582	403
		4	133.36	74985	432
		5	132.42	75517	407
		6	131.71	75924	
5	3.29	0	119.84	83444	420
		1	119.24	83864	410
		2	118.66	84274	422
		3	118.07	84696	403
		4	117.51	85099	
6	4.32	0	114.05	87681	432
		1	113.49	88113	430
		2	112.94	88543	409
		3	112.42	88952	421
		4	111.89	89373	
7	5.28	0	111.57	89630	411
		1	110.06	90041	423
		2	110.54	90464	
0				93560	

3.3. CH_2Cl_2

3.3.1. Photoabsorption

The photoabsorption cross section of CH_2Cl_2 measured with a monochromator resolution of 0.2 nm is shown in fig. 5. The current result agrees very well with the data of Russell et al. [3]. The absorption bands in the 130–200 nm region have been assigned to Rydberg transitions [3,8]. The assignment given by Robin [8] is indicated in fig. 5.

Vibrational structure appears in the absorption spectrum at wavelengths shorter than 145 nm. An attempt to classify these absorption bands into Rydberg series is not successful, instead, six vibrational progressions are classified as shown in fig. 6, which was measured with a monochromator resolution of 0.04 nm. The wavelengths, wave numbers, and vibrational frequencies for the tentatively classified vibrational progressions are listed in table 2. The vibrational progressions I and II have been observed by Zobel and Duncan

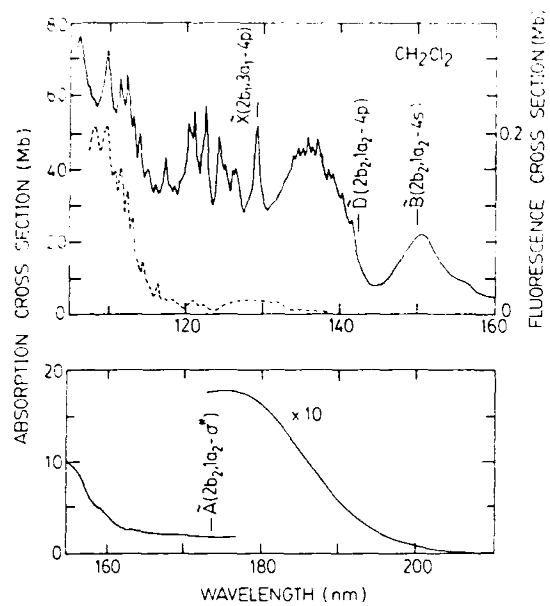

Fig. 5. Photoabsorption (———) and fluorescence (---) cross sections of CH_2Cl_2 measured with a monochromator resolution of 0.2 nm.

[19]. The progressions I, II, and VI have an average vibrational frequency of about 680 cm^{-1}, which is close to the ν_3 frequency (CCl_2 symmetrical stretching mode) of the ground state of CH_2Cl_2 (717 cm^{-1}) [18]. The vibrational progressions III, IV, and V have an average vibrational frequency of about 1000 cm^{-1}, which is close to the ν_5 frequency (CH_2 twisting mode) of the ground state of CH_2Cl_2 (1153 cm^{-1}) [18].

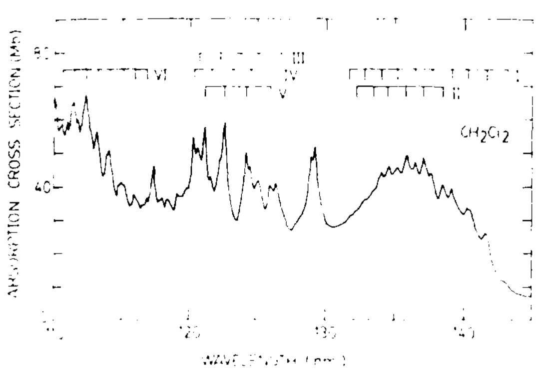

Fig. 6. Photoabsorption spectrum of CH_2Cl measured with a monochromator resolution of 0.04 nm. The wavelength positions for the tentatively assigned vibrational profgressions are indicated.

3.3.2. Fluorescence

The fluorescence cross section of CH_2Cl_2, which is simultaneously measured with the ab-

Table 2
Wavelengths, λ, wavenumbers, ν, and vibrational frequencies Δν, for the tentatively assigned vibrational progressions of CH_2Cl_2

Progression	v	λ (nm)	ν (cm^{-1})	Δν (cm^{-1})
I	0	143.00	69930	
	1	141.59	70626	696
	2	140.31	71270	644
	3	139.10	71890	620
	4	137.72	72611	621
	5	136.45	73287	676
	6	135.23	73948	661
	7	133.97	74644	696
	8	132.76	75324	680
	9	131.58	75999	675
II	0	138.43	72239	
	1	137.09	72945	706
	2	135.81	73632	687
	3	134.53	74333	701
	4	133.29	75024	691
	5	132.09	75706	682
III	0	126.79	78871	
	1	125.10	79936	1065
	2	123.74	80815	879
	3	122.14	81873	1058
	4	120.60	82919	1046
IV	0	126.35	79145	
	1	124.40	80386	1241
	2	122.99	81307	921
	3	121.53	82284	977
	4	120.26	83153	869
V	0	125.82	79479	
	1	124.11	80574	1095
	2	122.56	81593	1019
	3	121.10	82576	983
VI	0	116.81	85609	
	1	115.89	86289	680
	2	114.93	87009	720
	3	114.01	87712	703
	4	113.16	88370	658
	5	112.29	89055	685
	6	111.40	89767	712
	7	110.59	90424	657
	8	109.81	91066	642

sorption cross section, is shown in fig. 5. The fluorescence yield determined from the fluorescence cross section is shown in fig. 2c. Similar to CCl_4 and $CHCl_3$, the fluorescence yield shows two bands with maxima of 0.06% and 0.35% at 131 and 107 nm, respectively. The first band likely corresponds to a repulsive state (with a vertical energy of 9.5 eV) that dissociates into

$$CH_2Cl_2 \rightarrow CCl_2(\tilde{A}) + H_2. \quad (4)$$

The threshold of this process is calculated at 226 nm, using heat of formation of −21.19 kcal/mol for CH_2Cl_2 [9,10]. This calculated threshold wavelength is much longer than the fluorescence threshold wavelength observed at 137 nm.

The second band likely corresponds to the process

$$CH_2Cl_2 \rightarrow CCl_2(\tilde{A}) + 2H, \quad (5)$$

for which the threshold wavelength is 125 nm, where the dissociation energy of H_2 (4.4781 eV [11]) is used for the calculation. The calculated threshold for this second fluorescence band coincides with the observed threshold as shown in fig. 2c. The wavelength for the maximum yield of this band may occur at a wavelength shorter than 106 nm.

The $CH_2(\tilde{b}\,^1B_1-\tilde{a}\,^1A_1)$ emission, which has been observed from the photodissociative excitation of CH_4 [20], may be produced from the photoexcitation process

$$CH_2Cl_2 \rightarrow CH_2(\tilde{b}) + Cl_2. \quad (6)$$

The wavelength threshold for this process is expected to be 130 nm, as calculated from the heat of formation of 92.25 kcal/mol for CH_2 [9,10] and the excess energy of 4.63 eV required for the production of the $CH_2(\tilde{b}-\tilde{a})$ emission. This excess energy is assumed to be equal to the excess energy that produces the same emission from the excitation process of $CH_4 \rightarrow CH_2 + H_2$ [20]. The fluorescence yield for the $CH_2(\tilde{b} \rightarrow \tilde{a})$ emission is, however, expected to be quite small because the fluorescence yield for CH_3Cl is very small as discussed below.

3.4. CH_3Cl

The absorption cross section of CH_3Cl measured with a monochromator resolution of 0.04 nm is shown in fig. 7. The current result agrees with the data of Russell et al. [3] within experimental uncertainty. The absorption bands have been assigned to Rydberg transitions by several investigators [3,8,15,21]. The assignment given by Robin [8] is indicated in fig. 7. The sharp absorption bands have been classified into Rydberg series by Hochmann et al. [21].

The relative cross section for the production of fluorescence from photodissociative excitation of CH_3Cl is shown in fig. 7, where the data were measured with a resolution of 0.7 nm. The upper limit for the fluorescence cross section is estimated

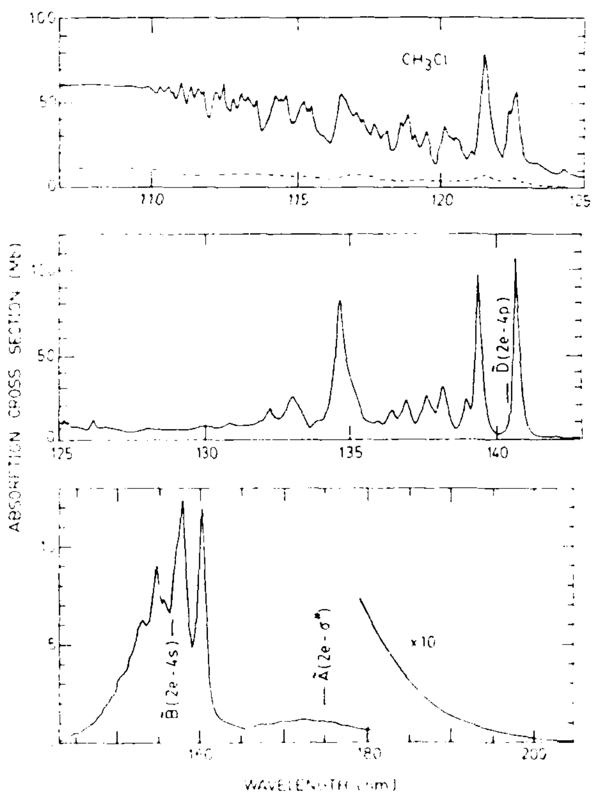

Fig. 7. Photoabsorption (———) and relative fluorescence (---) cross sections of CH_3Cl. The monochromator resolutions were 0.04 nm for the absorption and 0.7 nm for the fluorescence. The upper limit for the fluorescence cross section is estimated to be 10^{-20} cm^2.

to be 10^{-20} cm^2. The fluorescence cross section is quite small when compared with other chloromethane molecules. The fluorescence yield is smaller than 0.02% for the entire wavelength region studied. The fluorescence may mainly consist of the $CH_2(\tilde{b}-\tilde{a})$ emission, which is produced from the process,

$$CH_3Cl \rightarrow CH_2(\tilde{b}) + HCl. \quad (7)$$

The wavelength threshold for this process is 147 nm as calculated from the heats of formation of -22.019 and -18.1 kcal/mol for HCl and CH_3Cl, respectively [9,10], and the excess energy of 4.63 eV for the production of the $CH_2(\tilde{b}-\tilde{a})$ emission [20]. This calculated threshold is longer than the observed fluorescence threshold of about 124.5 nm.

4. Concluding remarks

The absorption and fluorescence cross sections of CCl_4, $CHCl_3$, CH_2Cl_2, and CH_3Cl are measured in the 105–220 nm region, and used to determine the fluorescence quantum yields. In general, the spectrum of each fluorescence yield shows two maxima, indicating that the fluorescence is produced by two repulsive states. The wavelength at the maximum fluorescence yield is used to determine the vertical energy of the repulsive state.

Robin [8,22] has assigned the intense energy loss band at 81000 cm^{-1} in the electron impact spectrum of CCl_4 to the $\sigma \rightarrow \sigma^*$ transition. This transition may correspond to the first fluorescence band of CCl_4 that has a maximum yield of about 1% at 130 nm as shown in fig. 2a. Similarly, the first fluorescence bands of $CHCl_3$ and CH_2Cl_2 as shown in figs. 2b and 2c could be assigned to the same transition.

Acknowledgement

The authors wish to thank the staff of the Synchrotron Radiation Center of the University of Wisconsin for their delicate operation of the facility. The synchrotron radiation facility is supported by the NSF under Grant No. DMR-44-21888. This work is based on the work supported by the NSF under Grant No. ATM-8412618 and CBT-8518555, the NASA under Grant No. NAGW-319, and the ONR under Grant No. N00014-86-K-0558.

References

[1] T. Ibuki, N. Takahashi, A. Hiraya and K. Shobatake, J. Chem. Phys. 85 (1986) 5717.
[2] G. Lucazeau and C. Sandorfy, J. Mol. Spectry. 35 (1970) 214.
[3] B.R. Russell, L.O. Edwards and J.W. Raymonda, J. Am. Chem. Soc. 95 (1973) 2129.
[4] G.C. Causley and B.R. Russell, J. Electron Spectry. 11 (1977) 383.
[5] H. Tsubomura, K. Kimura, K. Kaya, J. Tanaka and S. Nagakura, Bull. Chem. Soc. Japan 37 (1964) 417.
[6] L.C. Lee, J. Chem. Phys. 72 (1980) 4334.
[7] L.C. Lee and M. Suto, Chem. Phys. 110 (1986) 161.
[8] M.B. Robin, Higher excited states of polyatomic molecules, Vols. 1, 2 (Academic Press, New York, 1974).
[9] H. Okabe, Photochemistry of small molecules (Wiley, New York, 1978).
[10] D.R. Stull and H. Prophet, eds., JANAF thermochemical tables, 2nd Ed., NSRDS-NBS 37 (1971).
[11] K.P. Huber and G. Herzberg, Molecular spectra and molecular structure, Vol. 4. Constants of diatomic molecules (Van Nostrand–Reinhold, New York, 1979).
[12] D.A. Predmore, A.M. Murray and M.D. Harmony, Chem. Phys. Letters 110 (1984) 173.
[13] A.W. Potts, H.J. Lempka, D.G. Streets and W.C. Price, Phil. Trans. Roy. Soc. London A 268 (1970) 59.
[14] R.N. Dixon, J.N. Murrell and B. Narayan, Mol. Phys. 20 (1971) 611.
[15] S. Felps, P. Hochmann, P. Brint and S.P. McGlynn, J. Mol. Spectr. 59 (1976) 355.
[16] H.T. Wang, W.S. Felps and S.P. McGlynn, J. Chem. Phys. 67 (1977) 2614.
[17] G. Herzberg, Infrared and Raman spectra of Polyatomic molecules, Vol. 2 (Van Nostrand, New York, 1945).
[18] T. Shimanouchi, Tables of molecular vibrational frequencies, Consolidated Vol. 1, NSRDS-NBS 39 (1972).
[19] C.R. Zobel and A.B.F. Duncan, J. Am. Chem. Soc. 77 (1955) 2611.
[20] L.C. Lee and C.C. Chiang, J. Chem. Phys. 78 (1983) 688.
[21] P. Hochmann, P.H. Templet, H.T. Wang and S.P. McGlynn, J. Chem. Phys. 62 (1975) 2588.
[22] M.B. Robin, Higher excited states of polyatomic molecules (Academic Press, New York, 1985) pp. 109–110.

Appendix C

"Electron-Impact Ionization and Attachment Cross Sections of CH_3OH, NH_3, and CH_3Cl"

S. K. Srivastava, Jet Propulsion Laboratory

ELECTRON IMPACT IONIZATION AND ATTACHMENT TO RADICALS

S. K. Srivastava, Jet Propulsion Laboratory, 4800 Oak Grove Drive, Pasadena

PROGRESS REPORT FOR THE PERIOD Feb. 6, 1987 THROUGH Dec. 31, 1987.

The financial support to the present task started on February 6, 1986. Since then we have made the following progress:

1) Supplied to SDSU design drawings and other details for the fabrication of an "Electron Impact Ionization Spectrometer."

2) Visited SDSU four times and helped in the performance evaluation of the spectrometer.

3) Made measurements on the following molecules:

   i) Cross sections for the production of positive ions: NH_3, CH_3OH.

   ii) Attachment and dissociative attachment cross sections: $CH_3C\ell$, SiH_4 and CH_4.

   These cross sections are needed for normalization of data obtained for radicals.

The technical papers for publication will be written soon. However, the cross section data in tabular form and figures is attached here. Table I shows the cross section values for the production of various positive ions from NH_3. Figure 1 shows these cross sections. Figure 2 presents dissociative attachment cross sections for $CH_3C\ell$. Figures 3, 4, 5 and 6 give cross sections for the various radical negative ion species from SiH_4. Figure 7 shows the negative ion production cross sections from CH_4.

Cross Section for Positive Ions from Excitation of CH_3OH

at 100 eV Electron Energy

Ion Species		Cross Section ($\times 10^{-18}$ cm^2)
CH_3OH^+		113.16
CH_2CH^+	Standard	154.70
$CHOH^+$		12.35
CHO^+		93.45
CO^+		11.68
H_3O^+		0.469
H_2O^+		2.88
OH^+		2.02
O^+		1.20
CH_3^+		40.01
CH_2^+		6.50
CH^+		0.269
C^+		1.76
H_2^+		28.74
H^+		0.853

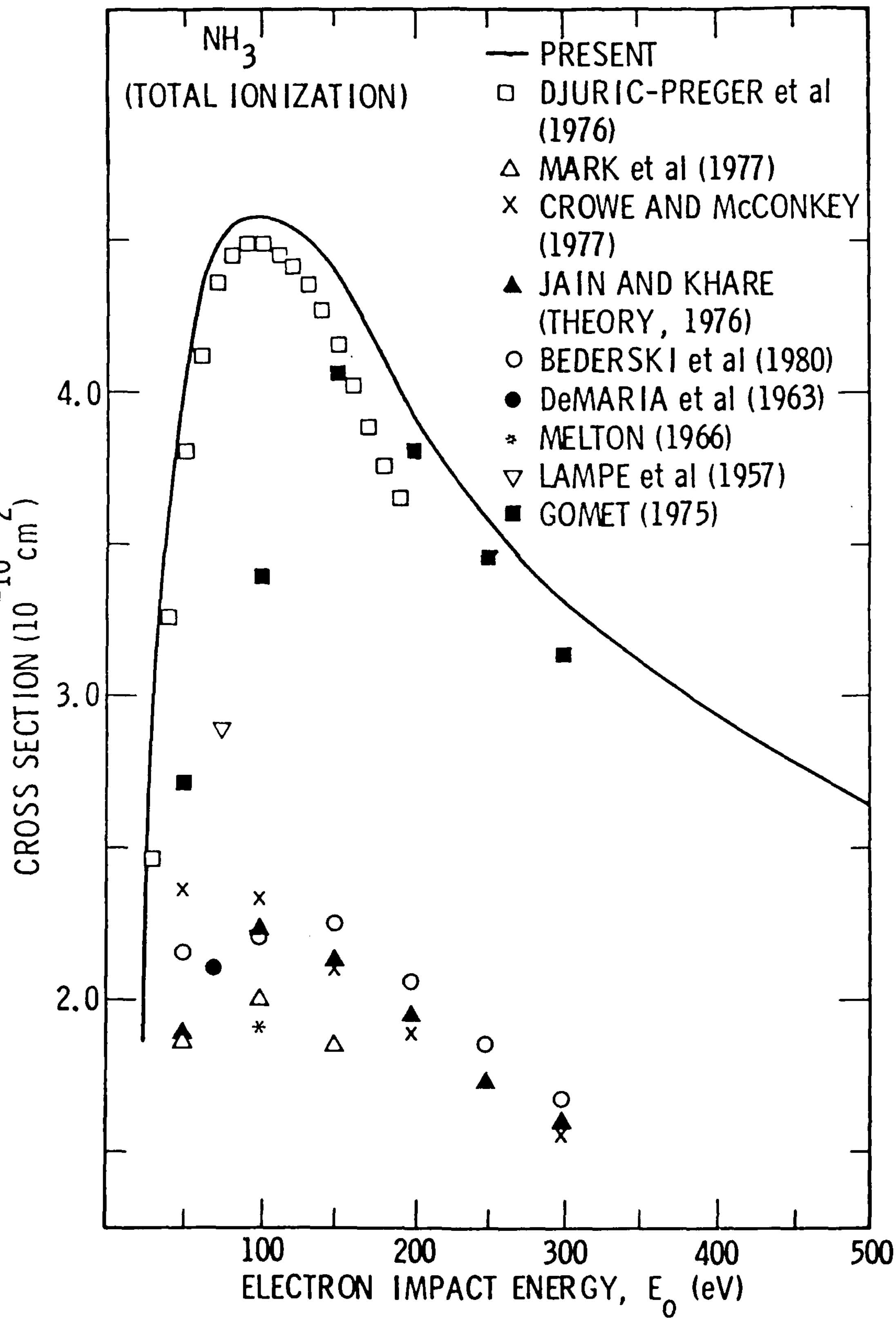

NH3
(TOTAL IONIZATION)
PRESENT
DJURIC-PREGER et al (1976)
MARK et al (1977)
CROWE AND McCONKEY (1977)
JAIN AND KHARE (THEORY, 1976)
BEDERSKI et al (1980)
DeMARIA et al (1963)
MELTON (1966)
LAMPE et al (1957)
GOMET (1975)
CROSS SECTION (10-16 cm2)
4.0
3.0
2.0
100
200
300
400
500
ELECTRON IMPACT ENERGY, E0 (eV)

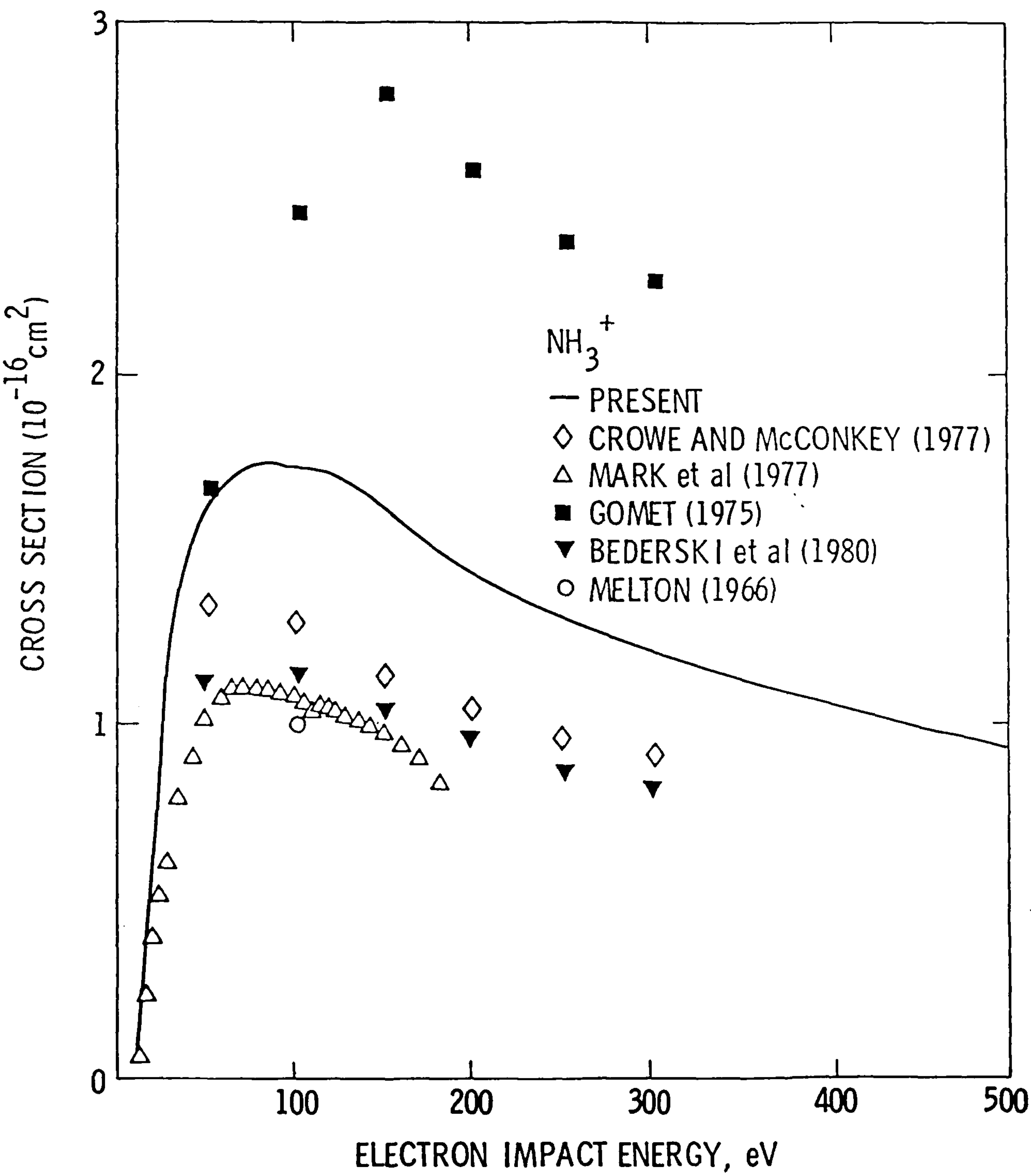

3
2
1
0
100
200
300
400
500
ELECTRON IMPACT ENERGY, eV
CROSS SECTION ($10^{-16}cm^2$)
NH_3^+
— PRESENT
◇ CROWE AND McCONKEY (1977)
△ MARK et al (1977)
■ GOMET (1975)
▼ BEDERSKI et al (1980)
○ MELTON (1966)

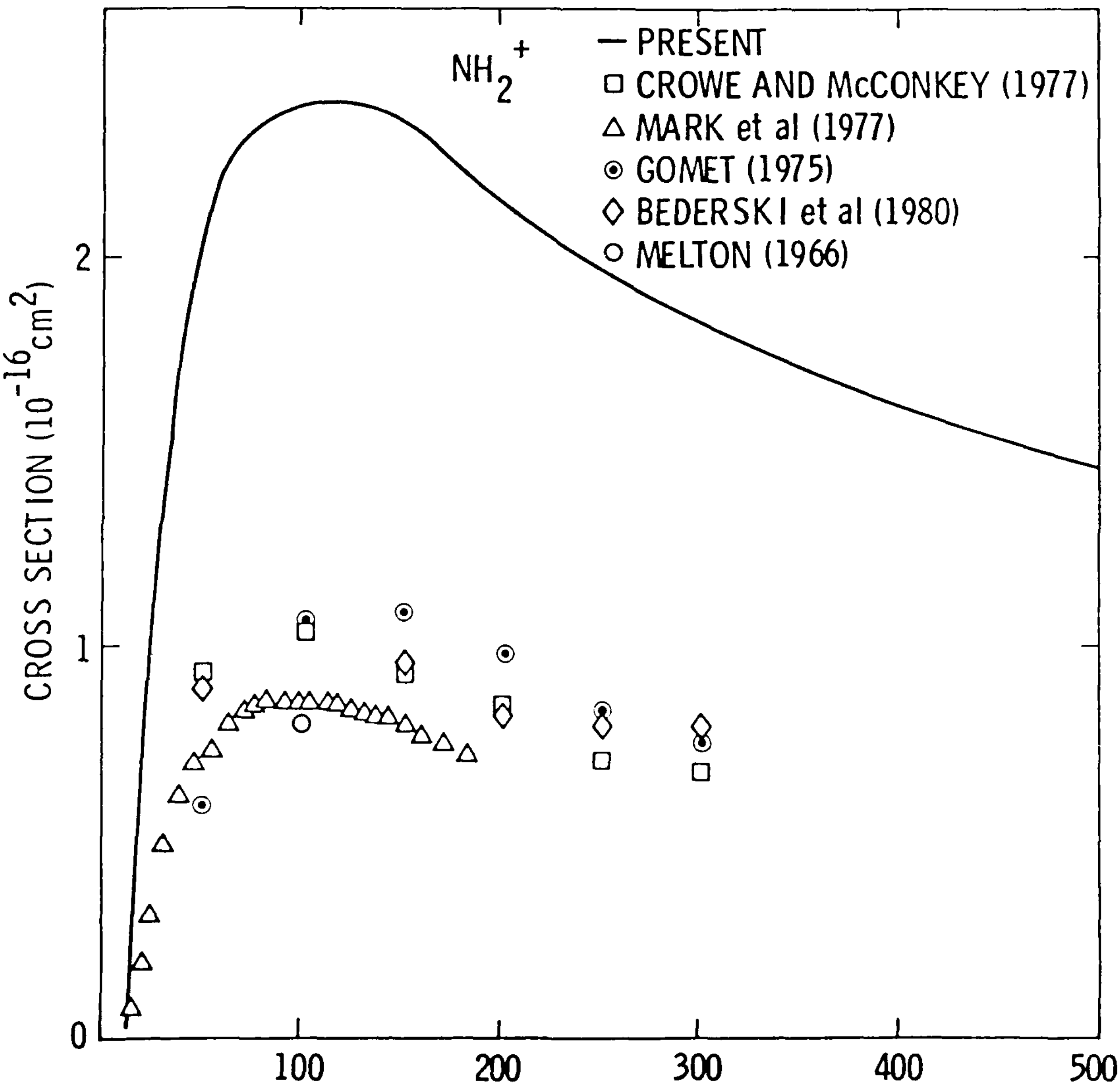

NH2+
— PRESENT
□ CROWE AND McCONKEY (1977)
△ MARK et al (1977)
⊙ GOMET (1975)
◇ BEDERSKI et al (1980)
○ MELTON (1966)
CROSS SECTION (10-16 cm2)
0
1
2
100
200
300
400
500
ELECTRON IMPACT ENERGY, eV

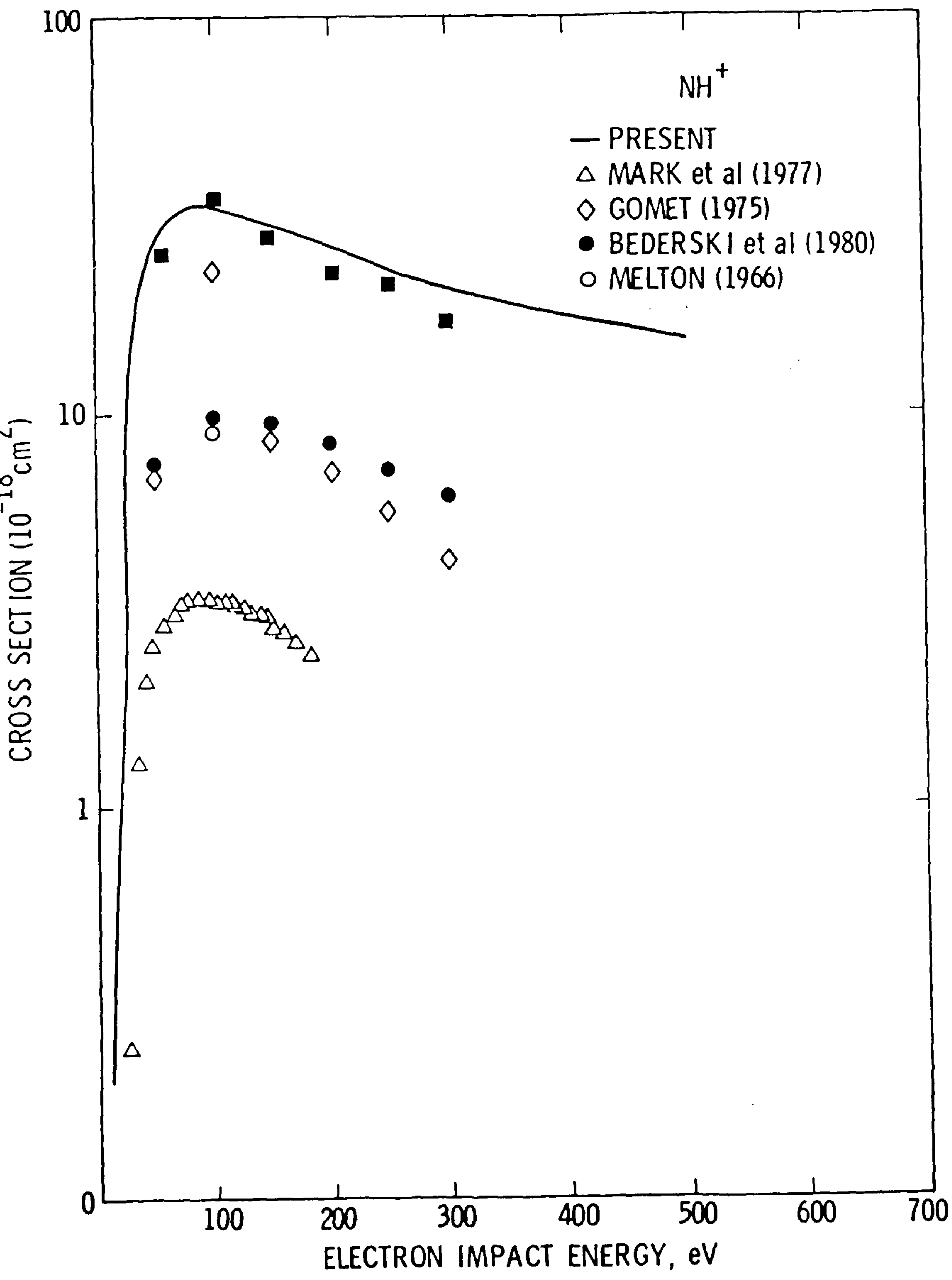
NH$^+$
— PRESENT
△ MARK et al (1977)
◇ GOMET (1975)
● BEDERSKI et al (1980)
○ MELTON (1966)
100
10
1
0
100
200
300
400
500
600
700
CROSS SECTION ($10^{-18}cm^2$)
ELECTRON IMPACT ENERGY, eV

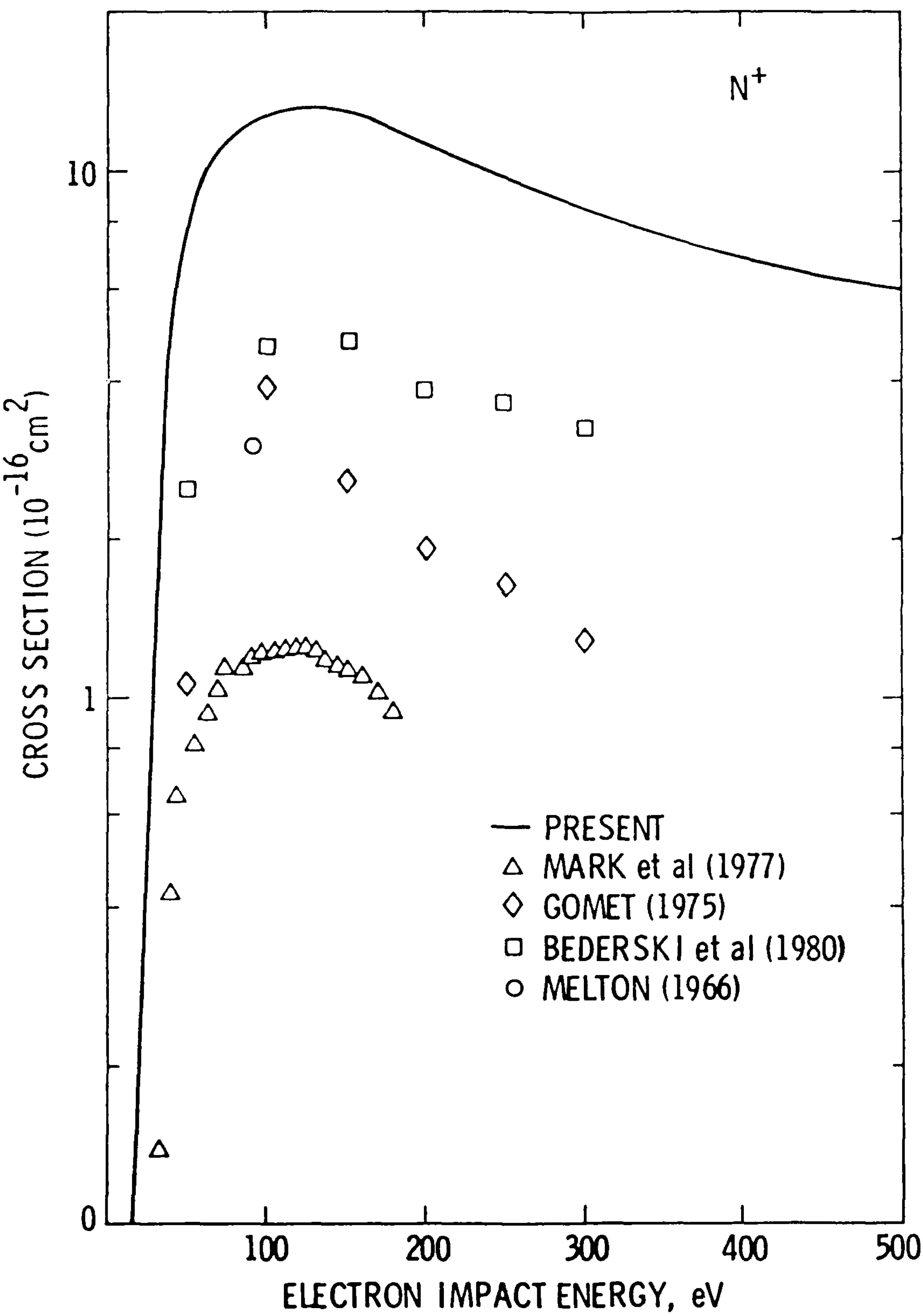
N+
10
1
0
CROSS SECTION (10^{-16}cm^2)
100
200
300
400
500
ELECTRON IMPACT ENERGY, eV
PRESENT
MARK et al (1977)
GOMET (1975)
BEDERSKI et al (1980)
MELTON (1966)

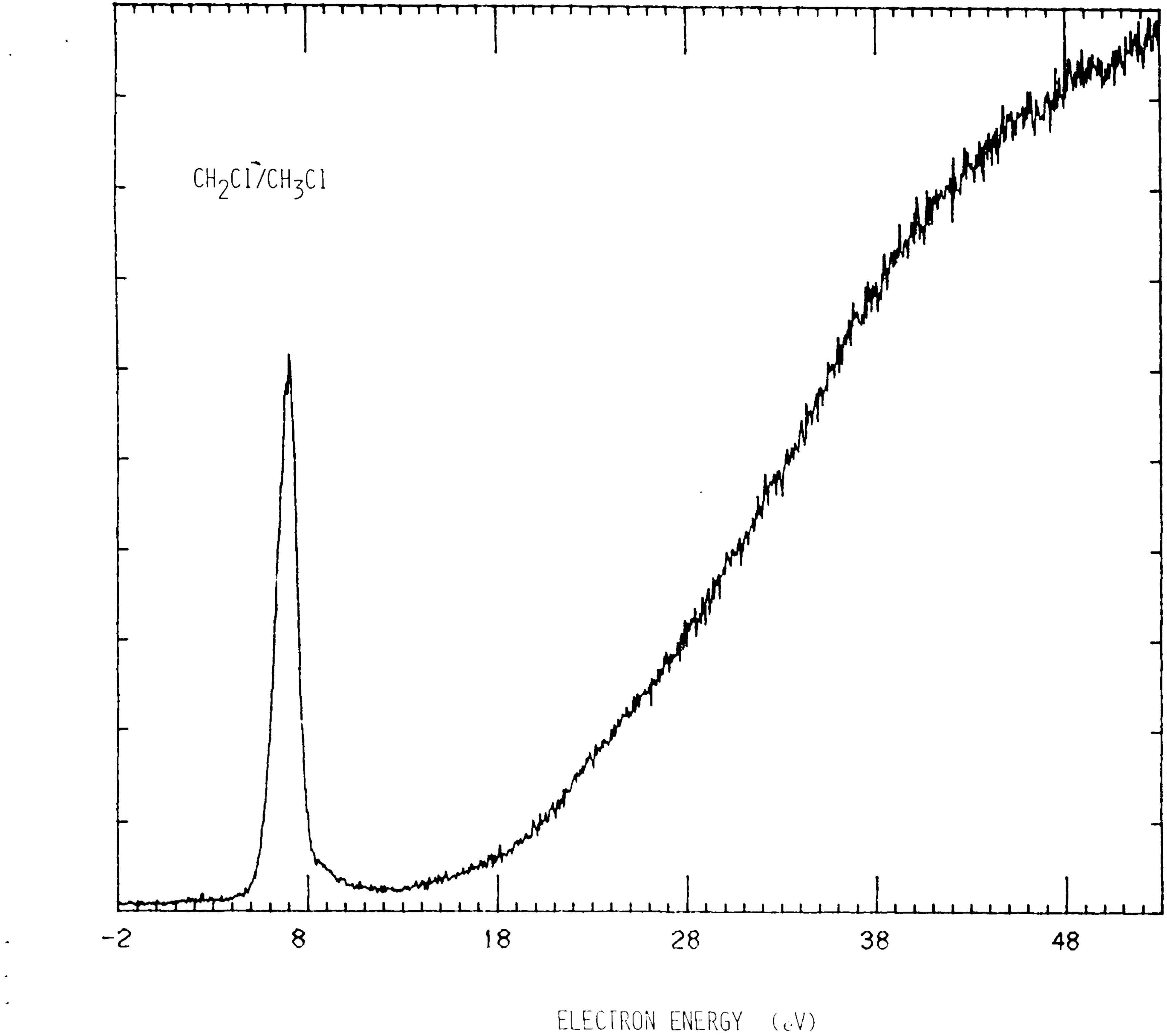

CH_2Cl^-/CH_3Cl
-2
8
18
28
38
48
ELECTRON ENERGY (eV)

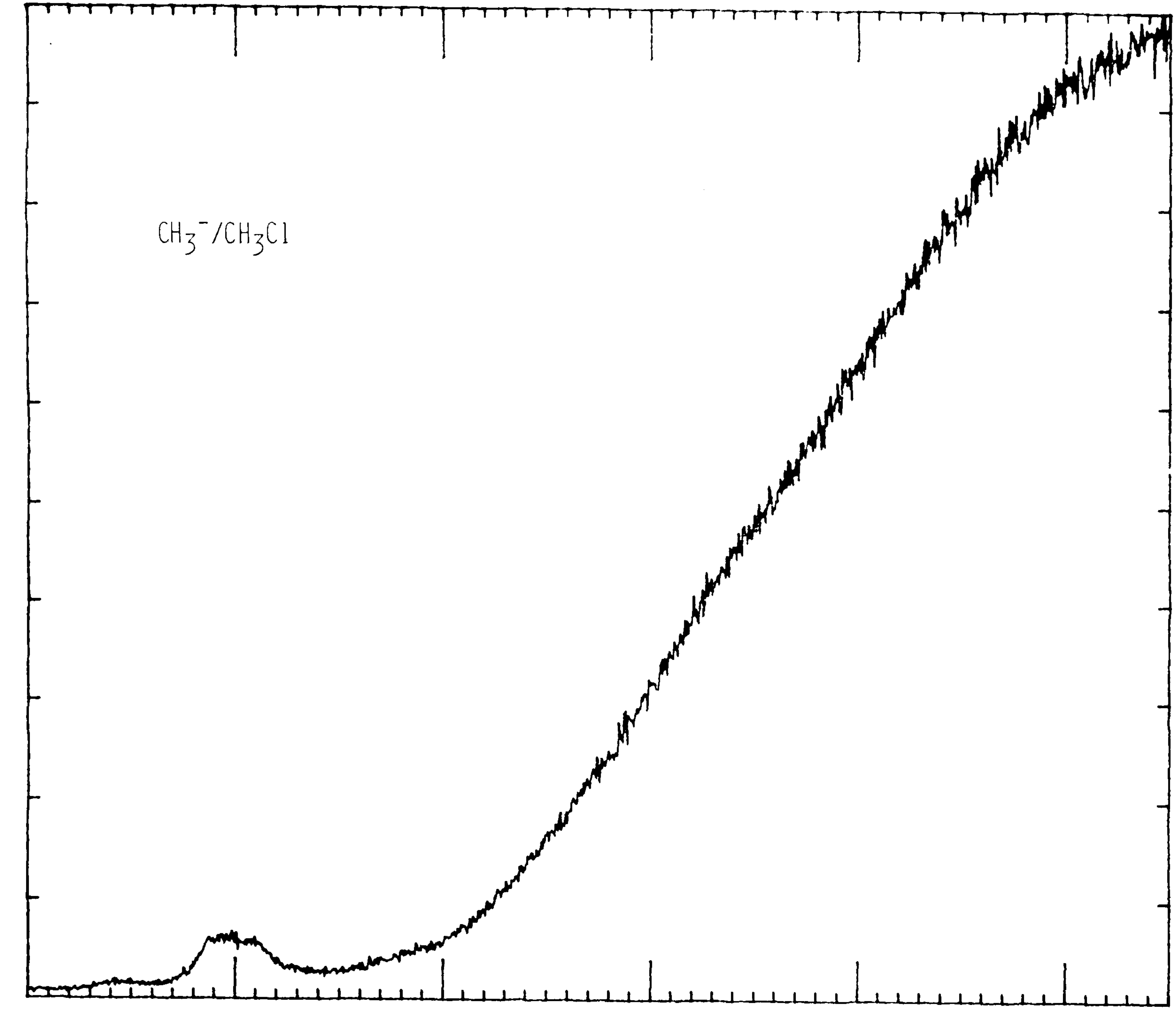
CH3⁻/CH3Cl
-2
8
18
28
38
48
ELECTRON ENERGY (eV)

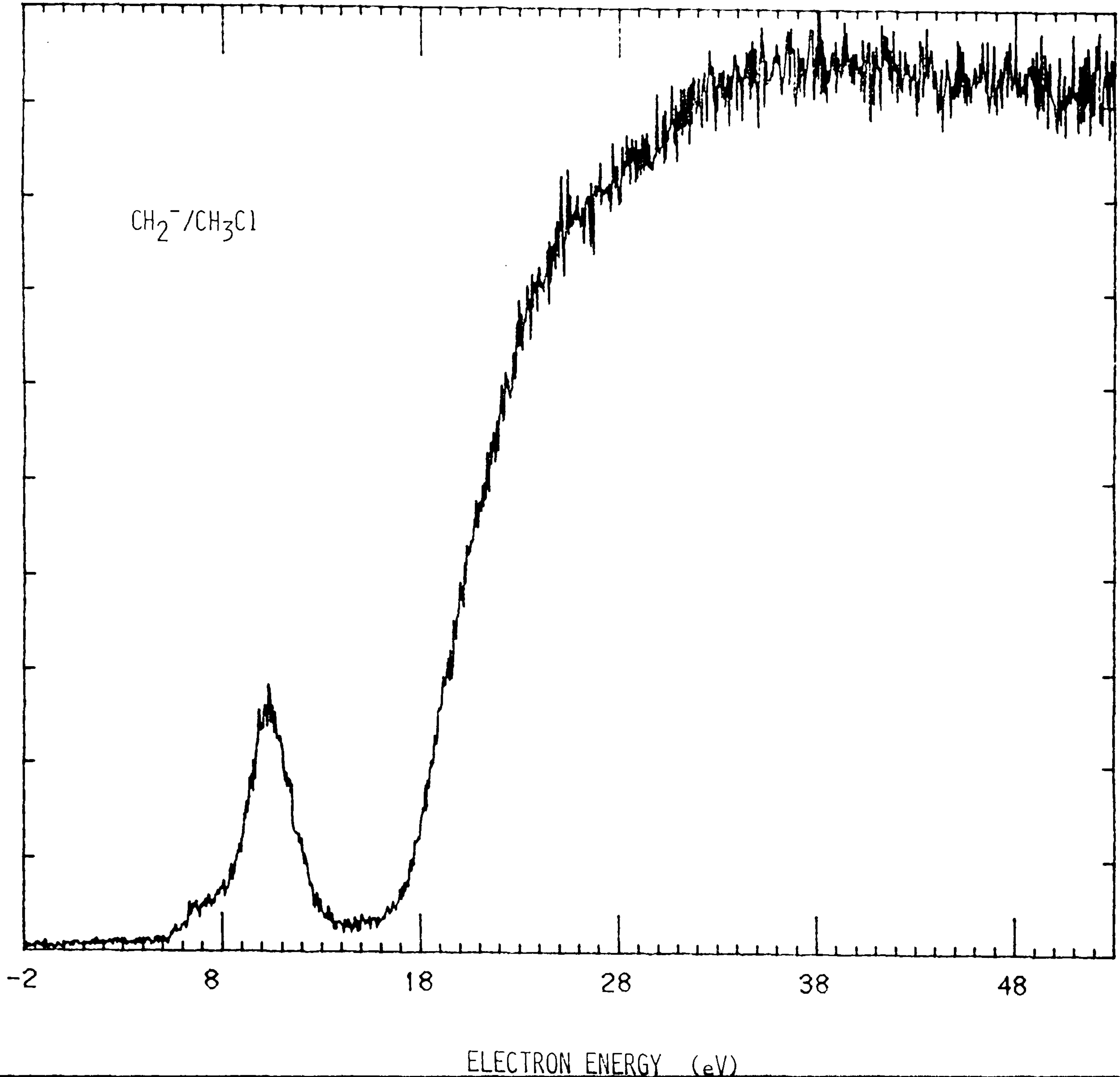

CH_2^-/CH_3Cl
-2
8
18
28
38
48
ELECTRON ENERGY (eV)

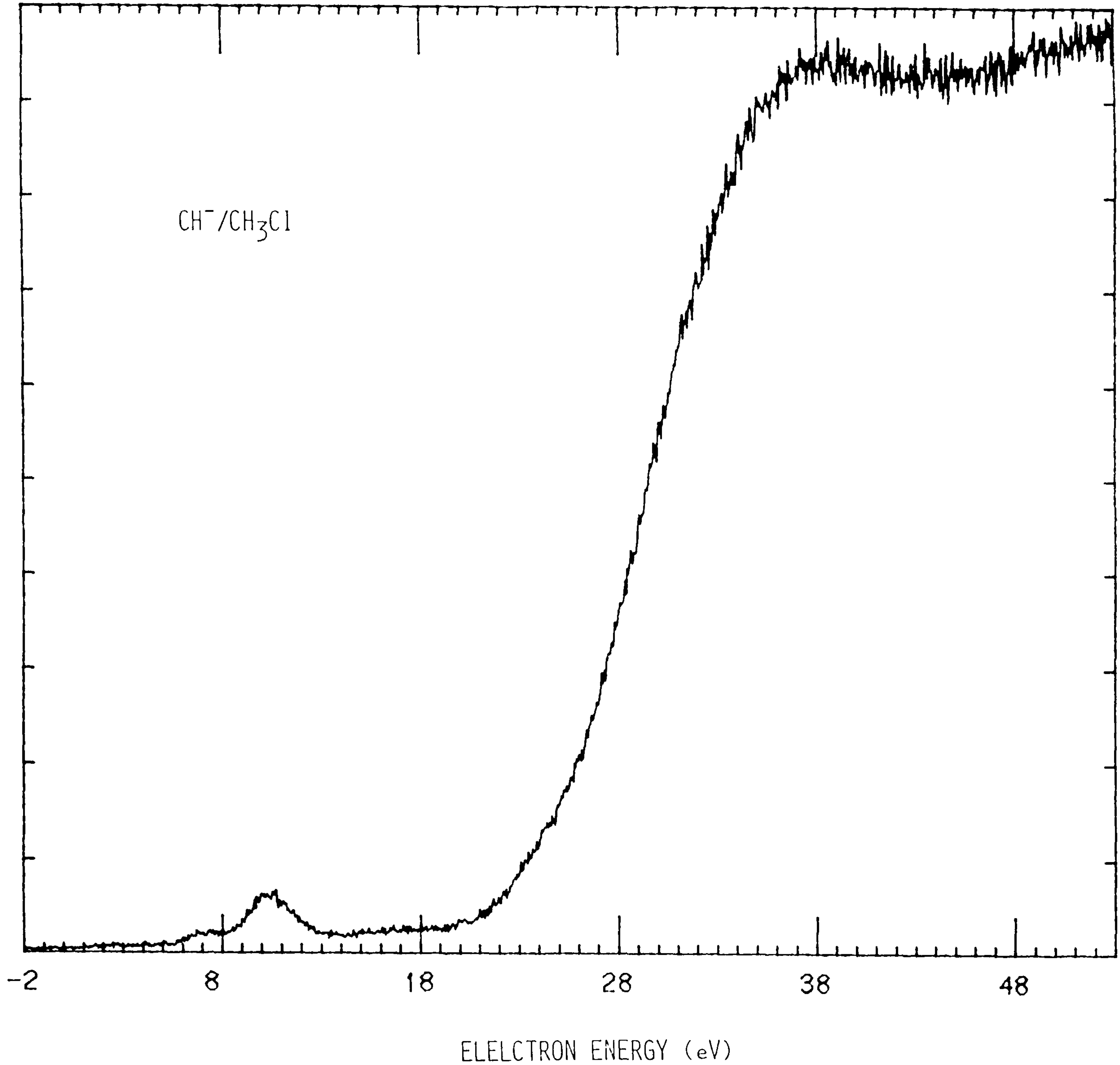

CH^-/CH_3Cl
-2
8
18
28
38
48
ELELCTRON ENERGY (eV)

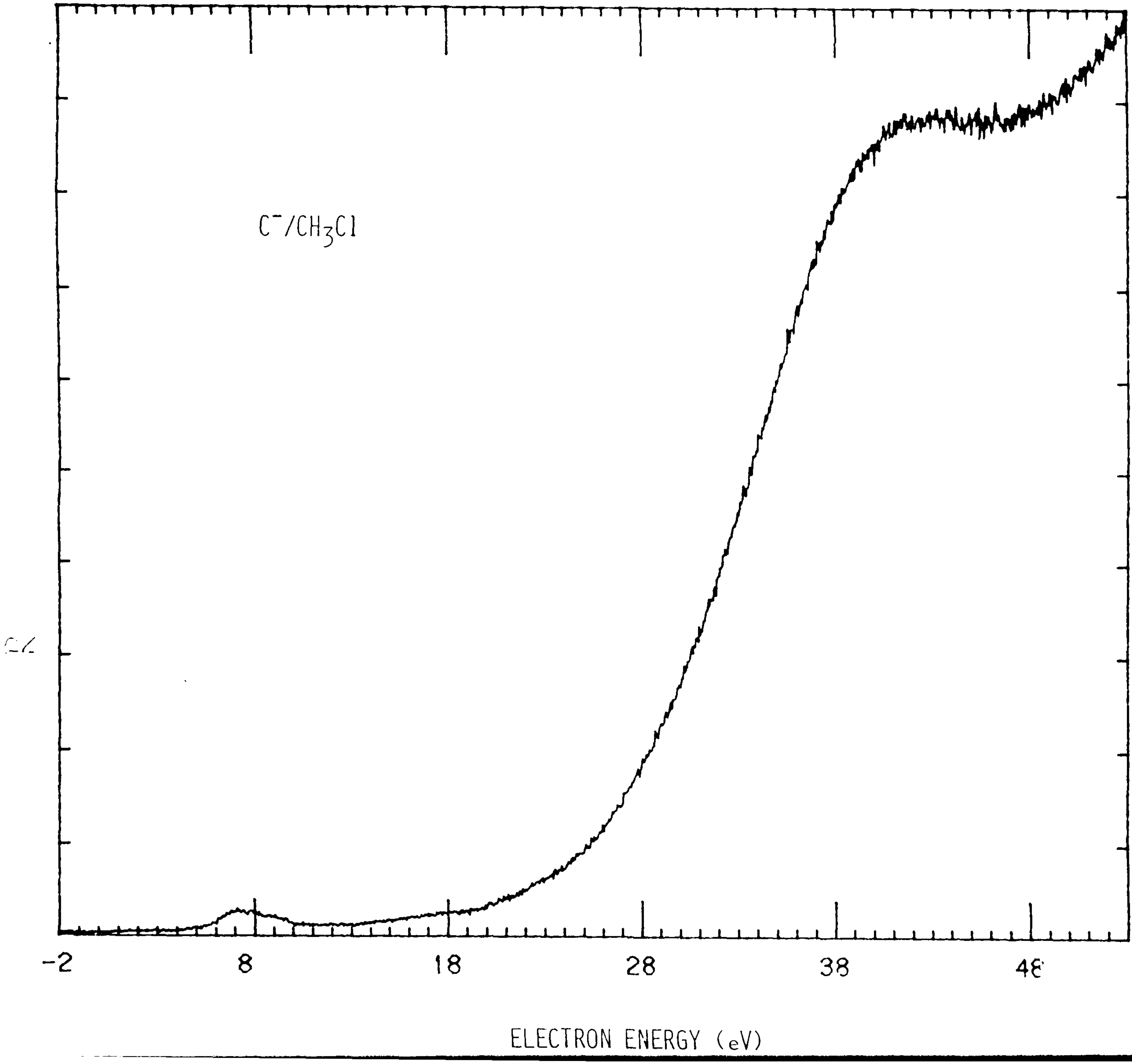

C⁻/CH₃Cl
-2
8
18
28
38
48
ELECTRON ENERGY (eV)

END
DATE
FILMED
6-88
DTIC